Persistent EarthCARE underflight studies of the ITCZ and organized convection (PERCUSION): Contribution to EarthCARE Validation

Silke Groß[1], Florian Ewald[1], Bjorn Stevens[2], Martin Wirth[1], Georgios Dekoutsidis[1], André Ehrlich[3], Dimitra Kouklaki[4], Konstantin Krüger[1], Sophie Rosenburg[3], Lea Volkmer[5], Jonas v. Bismark[6], Lutz Hirsch[2], Anna E. Luebke[3], Eleni Marinou[4], Bernhard Mayer[5], Montserrat Pinol Sole[6], Manfred Wendisch[3], Julia Windmiller[2], Vassilis Amiridis[4], Rob Koopman[6], Takuji Kubota[7], Markus Rapp[1]

[1]Institue of Atmospheric Physics (PA), German Aerospace Center (DLR), Oberpfaffenhofen, Germany

[2]Max Planck Institute for Meteorology (MPI-M), Hamburg, Germany

[3] Leipzig Institute for Meteorology (LIM), Leipzig University, Leipzig, Germany

[4] National Observatory of Athens (NOA), Athens, Greece

[5]Ludwig-Maximilians-Universität München (LMU), Munich, Germany

[6]European Space Agency (ESA), Noordwijk, Netherlands

[7]Earth Observation Research Center, Japan Aerospace Exploration Agency (JAXA), Tsukuba-city, Japan

Correspondence to: Silke Groß (silke.gross@dlr.de)

Abstract.

In May 2024, the Earth Clouds, Aerosols and Radiation Explorer (EarthCARE) satellite was launched. For the first time a satellite payload combines two active instruments, i.e., the Atmospheric Lidar and the Cloud Profiling Radar, together with two passive instruments, a multi-spectral imager and a broad-band radiometer, on one single spacecraft platform. EarthCARE is thus the most complex satellite mission to date for collocated aerosol, cloud, radiation and precipitation measurements. To utilize the data collected by the EarthCARE mission to its full extent and to support and quantify the data quality and measurement uncertainty, careful and holistic validation activities are needed. For this purpose, we set up an airborne instrument payload on the German High Altitude and LOng-range research aircraft (HALO), which is similar to the EarthCARE instrumentation. We used this payload during an extensive measurement campaign in summer and fall 2024 in the tropic and mid- to high-latitudes to validate the EarthCARE measurements and data products early in its commissioning phase. Here we aim to give a detailed overview of the PERCUSION (Persistent Earth CARE underflight studies of the ITCZ and organized convection) mission, and to advertise the use of its data in future more detailed validation studies. We give examples of how to use PERCUSION data to approach the validation of all for instruments of EarthCARE as well as of higher level (i.e. multi-sensor) products, and give first confidence in the quality of EarthCARE data.

1. Introduction

Despite major progress in understanding atmospheric aerosol and cloud processes and how they respond to changes in their environment are, given some scenario of forcing, still the largest source of uncertainty in climate change projections (IPCC, 2023). An important contribution to the global characterization of aerosol particles and clouds has been made by two satellite missions whose instruments focused on aerosol and cloud vertical profiling by lidar and radar, respectively; NASA's Cloud Aerosol Lidar Pathfinder Satellite Observation (CALIPSO) mission (Winker et al., 2010) and NASA's Cloudsat mission (Stephens et al., 2008). Launched jointly in 2006, they provided detailed information on the vertical structure of aerosol and cloud properties globally. Especially their synergistic use provided new insights that stimulated research on aerosol and cloud processes, and their interaction (Stephens et al., 2018). The benefit of the satellite missions could be ensured by extensive and repeated validation activities using complementary measurements throughout the lifetime of the mission.

Following the Committee on Earth Observation Satellites (CEOS) nomenclature, validation is defined as the process of assessing the quality of data products by independent means (ISO/TS 19159- 1:2014). This can include the assessment of the quality of the data products, the quality of the measurements themselves, and the representativeness of the data. The independent means are defined as data from instruments independent of those that provided the data products but measuring the same geophysical quantity as the satellite sensor whose data is to be validated. A review and summary of the general approaches, challenges and limitations for the validation of satellite missions (Langsdale et al., 2025) and with a focus on profiling missions (Amiridis et al., 2025) highlight the importance of trusted and comparable independent data.

Airborne measurements with the same or similar sensors as borne by the satellite have been shown to be a valuable tool for satellite validation, especially in the case of active sensors such as lidar (Gimmestad et al., 2017) and radar. For the validation of Cloud-Aerosol LIdar with Orthogonal Polarization (CALIOP) onboard of CALIPSO, a total of 147 underflights with an airborne high spectral resolution lidar (HSRL) were performed during the lifetime of the mission, which proved to have the most impact in measurement validation and algorithm improvement. These measurements were used to assess the quality of the CALIOP Level 1 products at the onset of the mission (Rogers et al., 2011), and provided quality assessments of algorithm improvements as the mission evolved (Getzewich et al., 2018; Kar et al., 2018). Airborne HSRL measurements were used to assess CALIOP Level 2 products, e.g., the aerosol particle backscatter and extinction coefficient, the optical depth, aerosol type classification, and the layer detection sensitivity (Burton et al., 2013; Kacenelenbogen et al., 2014; Rogers et al., 2014). To validate CALIOP and the Cloud Radar data, the CALIPSO and Cloudsat Validation Experiment (CC-VEX) took place immediately after the commissioning phase of both satellites (McGill, et al., 2007), deploying an elastic backscatter lidar and a W-band cloud radar on the ER-2 aircraft and NASA's HSRL (Hair et al., 2008) system on the Beechcraft B-200 King Air. During the Canadian Cloudsat-CALIPSO Validation Project airborne Ku-band radar measurements were performed for validation purposes (Barker et al., 2008). More recently, the lidar aboard ESA's Earth Explorer wind lidar mission AEOLUS likewise benefited from airborne validation campaigns (e.g., Lemmerz et al., 2023, Bedka et al., 2021; Witschas et al., 2020; Witschas et al., 2022). A large impact in the preparation (Lux et al., 2018) and the improvement of retrievals (Lux et al., 2022)

was made by the development and deployment of an airborne demonstrator of the spaceborne system (Reitebuch et al., 2009; Paffrath et al., 2009). Beyond the validation of active sensors, airborne demonstrators proved a valuable tool for passive satellite missions (King et al., 1996).

Motivated by the benefit of airborne demonstrators (Fix et al., 2016), and in particular the above mentioned activities for active systems designed to profile aerosol and clouds, we set up an EarthCARE (**Earth C**louds, **A**erosols and **R**adiation **E**xplorer) - like airborne payload (Stevens et al., 2019) on the German High Altitude and LOng-range research aircraft (HALO) (Krautstrunk and Giez, 2012) to contribute to EarthCARE validation activities. Independently of EarthCARE we could use data collected by HALO to develop independent algorithms, e.g., its lidar-based aerosol type classification (Groß et al., 2013; Groß et al., 2015), aerosol type separation (Gutleben et al., 2022), lidar-radar target classification (Marinou et al., 2020). Furthermore, we developed and tested synergistic radar-lidar retrievals to derive ice and mixed-phase cloud microphysical properties (Cazenave et al., 2019; Aubry et al., 2024). We devised methods to improve the radiative transfer calculations for scenes including aerosol particles (Gutleben et al., 2019) and ice clouds (Ewald et al., 2021; Röttenbacher et al., 2024) to achieve consistency of corresponding radiative transfer simulations and precise spaceborne radiative budget measurements. Furthermore, we used these synergistic EarthCARE-like measurements to prepare for the use and the validation of data collected by EarthCARE by investigating the impact of measurement sensitivity, wavelength combination, attenuation and instrument characteristics on the derived data products (Delanoë et al., 2020; Groß and Ewald, 2018). For that, we conducted dedicated HALO underflights with this payload closely coordinated CALIPSO and Cloudsat (Schäfler et al., 2018, Stevens et al., 2019). Furthermore, we also used HALO together with the French SAFIRE Falcon and at a later stage ATR-42 as a Tandem Platform (Delanoe et al., 2014). Our experiences supported the formulation of recommendations in a document for the best practices of validation for aerosol, cloud, and precipitation profiles (Amiridis et al., 2025).

These efforts contributed to the design of the PERCUSION (Persistent EarthCARE underflight studies of the ITCZ and organized convection) campaign, as a component of a broader field study ORCESTRA (Organized Convection and EarthCARE Studies over the Tropical Atlantic) (Stevens et al., 2026). Here we give an overview of the PERCUSION campaign with a focus on the validation of EarthCARE measurements. This includes: addressing the requirements and needs for EarthCARE validation (Section 2) and in Section 3 a description of the instrumentation and measurement strategy deployed for EarthCARE validation activities. In Section 4 we show some examples to illustrate the potential of PERCUSION EarthCARE data-product validation. Finally, we conclude (Section 5) with a discussion of our findings and the potential for the use of the measured dataset, not only for EarthCARE but also for other satellite missions.

2. Requirements for EarthCARE Validation

With the launch of the EarthCARE satellite in May 2024, the most complex Earth Explorer Missions to date started to measure aerosol and clouds, and their interactions and impacts on precipitation and the radiative energy budget (Wehr et al., 2023). EarthCARE, a joint mission of the European Space Agency (ESA) and the Japan Aerospace Exploration Agency (JAXA),

combines four instruments on a single polar orbiting platform. The Atmospheric LIDar (ATLID), the Multi-Spectral Imager (MSI), and a BroadBand Radiometer (BBR), are developed by ESA, and the Cloud Profiling Radar (CPR) is jointly developed by JAXA and the National Institute of Information and Communications Technology (NICT). The two active remote sensing instruments, the ATLID and the CPR, provide measurements of the vertical profiles of aerosol and cloud properties along the satellite track. The two passive remote sensing instruments, the MSI (which scans) and the BBR, provide the scene context information and measurements of the broadband radiation to estimate the net effect of the scene on Earth's radiant energy budget. To quantify the measurement uncertainties and data product quality, a thoughtful and holistic validation is needed. A general approach for EarthCARE validation is given in the EarthCARE Scientific Validation Implementation Plan (VIP) of ESA (Koopmann, 2024), which is adapted and refined in the validation strategy of the EarthCARE Data Innovation and Science Cluster (DISC; ESA, 2024). This strategy includes the outcome of a joint activity of the ESA EarthCARE Mission Advisory Group and instrument developers, which defines validation needs and target scenes of importance for EarthCARE validation (Hall, 2025). The aim is to provide information about the performance of EarthCARE data and retrievals in different synoptic regimes and for typical cloud and aerosol conditions.

2.1. Properties and Products

EarthCARE data are categorized according to data processing level (Table 1). The calibrated instrument data (Level 1b) for the three European instruments are provided by ESA, and for the CPR by JAXA. For higher level products, each Agency has its own processing chain. In this study we focus on the ESA processing chain. The data of the specific instruments are first processed individually (Level 1b and Level2a), and in a next step two or more instruments are processed in a synergistic way (Eisinger et al., 2024) to derive Level 2b data.

Table 1: EarthCARE Product Levels adopted from (Koopmann, 2024).

Level 0 Product	Raw instrument data, with duplicates removed and quality flags. For expert users only.
Level 1b Product	Instrument data processed to physical units, with error bars, quality flags and geolocations.
Level 1c Product	MSI only: Level 1b data re-sampled onto the grid of one selected MSI reference channel.
Level 1d Product	Auxiliary products.
Level 2 Product	Derived geophysical variables, with error bars, quality flags and geolocations.
Level 2a Product	Level 2 product derived from one single EarthCARE instrument
Level 2b Product	Level 2 product synergistically derived from two or more EarthCARE instruments

The ESA product chain generates 44 EarthCARE data products introduced by Eisinger et al. (2024) and references therein. JAXA's Level 2 algorithms for EarthCARE from single instrument to four sensor synergistic retrievals are described by Okamoto et al. (2024) and references therein. Besides the validation of the measurements (Level 1b) and the instrument data

in geophysical units (Level 2), specific needs for validation have been defined addressing the macrophysical properties as well as higher level products (ESA, 2023). They are summarized in Table 2.

Table 2: Needs for EarthCARE validation adapted from the EarthCARE Mission Advisory Group and developers (ESA, 2023) to be addressed by PERCUSION measurements.

Uncertainty	**Location/scene regimes**	**Instrument/Products**
Macrophysical properties		
Aerosol layer detection and type classification	• Multi-layer aerosol scenes • Strong internal layering	ATLID and ATLID-MSI Target Classification
Aerosol/cloud discrimination	• Cloud embedded in aerosol layers	ATLID and ATLID-MSI Target classification and layer product
Cloud layer detection	• Multi-layer aerosol/cloud scenes • Cirrus cloud over liquid cloud • Non-precipitating liquid clouds	MSI, ATLID, CPR layer detection and target classification
Cloud phase discrimination	• Multi-layer cloud scenes • Mixed-phase cloud scenes • Liquid clouds above ice clouds	MSI, ATLID, CPR target classification and feature mask
CPR surface clutter removal	• Measurements over different surface types	CPR Feature Mask
Ice cloud and snow		
Snow microphysics	• Stratiform and convective systems	CPR cloud product and synergistic cloud retrieval
Ice microphysical properties	• Different cloud types with a variety of temperatures, locations	ATLID ice cloud product and synergistic cloud retrieval
Rain		
Melting layer structure and attenuation of CPR	• Heavy precipitation events • Convective and stratiform systems	CPR cloud products and synergistic cloud retrieval
Aerosol		
AOT over land and sensitivity to aerosol classification	• Different land surfaces • Different aerosol types	MSI aerosol optical thickness

2.2. Target Scenes

The aim of the target scene is to include validation activities, which provide information about the performance of EarthCARE data and retrievals for different cloud and aerosol conditions, as summarized below:

- **Mixed aerosol types (MAT)**: To investigate the performance of ATLID across types and concentrations, including mixed and multi-layer scenes, and for different noise conditions (e.g. performance at daytime conditions compared to night-time conditions).
- **Cumulus and marine aerosol (CMA)**: Shallow, drizzle-free and often optically thin cumulus clouds are challenging to characterize from satellite observations (Mieslinger et al, 2022). They are difficult to detect by the CPR, but it is important to accurately mask them for ATLID aerosol retrievals, especially of marine aerosol particles.
- **Marine stratocumulus (MSC)**: The detection of marine stratocumulus can be challenging for satellite retrievals, and like for shallow cumulus, they often fall below the CPR detection threshold. Often a multi-sensor approach for their detection is applied. Measurements of the solar radiance provide optical constrains during the day (descending orbit). The evaluation of EarthCARE's performance to infer the location of marine stratocumulus, its cloud base and vertical extent and the profile of the liquid water path is important.
- **Large-scale rain (LSR)**: To evaluate how accurate rain rates can be retrieved from CPR, large scale rain conditions have to be addressed in the comparisons. It affects the CPR measurements e.g. by attenuation due to rain.
- **Snow, including snow above the melting layer (SML)**: Snow and snow over ice are common features in mid-latitude weather systems and thus important for validation. Their multi-layer structure (e.g. also including embedded supercooled liquid layers) makes it challenging to properly identify and retrieve.
- **Cirrus (CC)**: As compared to other cloud types, the impact of cirrus clouds on the radiative energy budget depends strongly on their optical and geometrical thickness. It is thus of importance to properly determine layer boundaries as well as optical and microphysical properties.
- **Complex multi-layer scenes (CLS)**: Multi-layer scenes are common in almost all synoptic regimes. A valid determination, separation and classification of the different layers are crucial to determine the overall radiative effect of the scenes. Combined radar and lidar measurements are often needed to determine different cloud types and to distinguish aerosols and clouds.
- **Deep convection (DC)**: Deep convection is challenging to properly investigate from satellite measurements, because it usually is accompanied by all cloud types and thus compounds many of the issues discussed above.

3. PERCUSION

PERCUSION is an initiative of the German research community had two main objectives:

(1) To test factors hypothesized to influence the organization of deep maritime convection in the tropics and the influence of organized convection on the large-scale environment, and

(2) Provide measurement for the validation of EarthCARE data products.

Measurements were performed in close collocation with EarthCARE during the period from August to November 2024. This manuscript mostly describes activities related to point (2). The motivation for and activities related to the first point are discussed in a complementary manuscript by Windmiller et al. (2026).

3.1. HALO and instrumentation

HALO is a modified Gulfstream G550. With a maximum cruising altitude of up to 15 km and a range of up to 10,000 km (~10 flight hours) it provides the capability for long and high flights, enabling extensive measurements over remote regions, which makes HALO well suited for satellite validation. During PERCUSION, HALO was equipped as a flying cloud observatory (Stevens, et al., 2019) combining active and passive remote sensing instrumentations, i.e., a high spectral resolution and depolarization sensitive lidar system, and a cloud radar with doppler capability, together with imager and radiation measurements (Table 3). In this configuration, HALO carries the most complete payload to mimic EarthCARE measurements. A large number of dropsondes (Stevens, et al., 2025; Gloeckner et al., 2025) provided profiles of the meteorological context. And measurements taken by instrumentation installed in the nose boom setup of HALO complemented crucial information on high-resolution thermodynamic and dynamic (wind) parameters at flight altitude. Table 3 provides a detailed summary of the HALO instrumentation and available products from the PERCUSION campaign.

Table 3: Detailed information on HALO instrumentation during PERCUSION. Adapted from (Stevens et al., 2019).

Instrument	**Institution**	**Observable**	**Derived products**
HAMP (HALO Microwave Package) Radiometers (Mech et al., 2014)	MPI-M, University Hamburg, University of Cologne, DLR-PA	Brightness temperature at 26 selected microwave frequencies between 22 and 183 GHz	• Integrated Water vapor • Temperature + humidity
HAMP Doppler Cloud radar MIRA (Ewald et al., 2019)	DLR-PA, MPI-M, University Hamburg	Profiles of radar reflectivity, depolarization ratio & Doppler velocity	• Cloud, snow • Target classification • Cloud geometry
WALES (Water vapor lider experiment in space) (Wirth et al., 2009)	DLR-PA	Profiles of • Atmospheric backscatter ratio at 532 nm, 935 nm and 1064 nm • Particle linear depolarization ratio at 532 nm • Particle extinction coefficient at 532 nm	Profiles of • Water vapor mixing ratio • Cloud mask • Aerosol classification • Extinction-to-backscatter ratio
specMACS (spectrometer of the Munich Aerosol Cloud Scanner) (Ewald et al., 2016; Weber et al., 2024)	LMU München	• Upward spectral radiance (400 – 2500 nm) with across-track field-of-view of 35° at a sampling rate of 30 Hz • Polarized radiance at RGB color channels, 2D fields (91° x 220°) at 5Hz sampling rate	• Cloud mask • Cloud phase • Cloud optical thickness • Effective particle size • Particle size distribution

BACARDI (Broadband AirCrAft RaDiometer Instrumentation) (Ehrlich et al., 2023)	Leipzig University	Upward and downward broadband irradiances • Solar (0.3 -3 µm) • Thermal-infrared (3-100 µm)	• Radiative energy budget • Cloud radiative effect • Heating and cooling rates
SMART (Spectral Modular Airborne Radiation Measurement System (Wendisch et al., 2001; Wolf et al., 2020)	Leipzig University	• Spectral upward and downward irradiance (300-2200 nm) • Spectral upward radiance (300-2200 nm)	• Spectral solar radiative energy budget • Cloud optical thickness • Liquid water path, effective particle size • Cloud thermodynamic phase
VELOX (Video airbornE Longwave Observations within siX channels) (Schäfer et al., 2022)	Leipzig University	Two dimensional fields of brightness temperature in 6 channels between 7.7 µm and 12.0 µm with 100 Hz temporal and 640 x 512 pixel resolution (field-of-view of 35.5° x 28.7°)	• Cloud mask, phase • Cloud top temperature • Cloud top altitude • Surface temperature
Dropsondes	MPI-M, DLR-PA, University Hamburg	Profiles of • Relative humidity • Temperature • Horizontal wind	
BAHAMAS (Basic Halo Measurement and Sensor System) (Giez et al., 2023)	DLR Flight experiment facility	In-situ observations of T, q, u, v, w, 100 Hz data navigational data, GPS, flight attitude	

3.2. Data analysis

Here we describe independent retrievals developed to derive similar data products from HALO as those from EarthCARE. This includes a lidar based aerosol classification (Groß et al., 2013; Groß et al., 2015) that was extended to include cloud radar measurements for a full target classification (Marinou, et al., 2020), as well as a method to derive cloud and aerosol layer heights and area (Groß et al., 2014; Dekoutsidis et al., 2024; Gutleben et al., 2019a). The airborne radar is calibrated (Ewald et al., 2019) and the measurements are analyzed. Subsequent of the basic analysis of both active remote sensing measurements, the data are used in a variational retrieval (Delanoë and Hogan, 2008; Cazenave et al., 2019) to derive higher level products; e.g., ice water content and ice effective radius. This retrieval was further developed to consider mixed-phase clouds and layers of super-cooled liquid water (Aubry et al., 2024). Aerosol and cloud optical and microphysical properties are used to calculate their radiative properties, e.g., heating rate profiles, top of the atmosphere radiances, and spectral radiance of clouds using the library for radiative transfer – libRadtran (Mayer and Kylling, 2005; Emde et al., 2016; Gutleben et al., 2020; Ewald et al., 2021), which can be directly compared to spectral radiance measured onboard HALO (Ewald et al., 2021) or to radiation measurements provided by EarthCARE. The specMACS data are used to determine cloud top height and geometry using a stereographic algorithm (Kölling, et al., 2019; Volkmer, et al., 2024). Cloud phase (Ehrlich et al., 2008; Weber, et al., 2025)

and cloud droplet radius (Pörtge, et al., 2023) are determined with high accuracy and high spatial resolution from the polarimetric angular observations. The thermal-infrared imager VELOX and the broadband radiometer BACARDI are radiometrically and geometrically calibrated as described by Ehrlich et al. (2023) and Schäfer et al. (2022). Atmospheric corrections based on radiative transfer simulations using the radiosonde measurements and the EarthCARE auxiliary data products are applied to the VELOX and BACARDI measurements. These corrections adjust the measurements at HALO flight level to top-of-atmosphere (TOA) brightness temperatures and broadband radiative fluxes comparable to MSI and BBR observations. Table 4 gives an overview of the EarthCARE in-orbit data products that can be validated with the PERCUSION measurements.

Table 4: EarthCARE in-orbit data products addressed for validation by PERCUSION

Earth CARE Products	
Level 1	MSI*
	ATLID
	CPR
Target classification	Cloud-top height
	Cloud-top phase
	Aerosol layer height/depth
	Aerosol layer classification
	Cloud detection, Cloud aerosol discrimination
	Cloud/precipitation fraction
	Cloud/precipitation phase
	Aerosol fraction
	Aerosol species
Ice cloud & snow	Optical thickness
	Effective radius
	Ice water path
	Extinction
	Extinction-to-backscatter ratio
Aerosol (per species)	Aerosol optical thickness
	Aerosol extinction
	Extinction-to-backscatter ratio

	Particle linear depolarization ratio
Radiation	BBR-SW unfiltered radiances
	Solar top-of-atmosphere flux
	Terrestrial top-of-atmosphere flux

*Despite the fact that both MSI on EarthCARE and specMACS and VELOX on HALO provide across-track coverage, only the exact nadir views can be compared since off-nadir observations from the EarthCARE orbit and the HALO flight altitude don't coincide spatially.

3.3. Measurement strategy

To achieve the objectives of PERCUSION, measurements were performed out of three locations to span the latitude range of what could broadly be called the Atlantic sector north of the Equator (Figure 1):

- **Eastern tropical Atlantic (Sal, Cape Verde)**: From 8 August to 5 September 2024 HALO flights were carried out of Sal (Cape Verde). This period provided the possibility for coordination with the French EarthCARE airborne validation activity within the MAESTRO (Mesoscale organisation of tropical convection) campaign and with validation activities of the Norwegian-Romanian validation activities (CELLO; Cloud and EarthCARE caL/vaL Observations), as well as with ground-based ACTRIS (The Aerosol, Clouds and Trace Gases Research Infrastructure) validation measurements from TROPOS at Minedlo (CLARINET; CLoud and Aerosol Remote sensing for EarThcare), and with shipborne measurements onboard the German Research Vessel (RV) Meteor (BOWTIE; Beobachtung von Ozean und Wolken – Das Trans ITCZ Experiment (Klocke et al., 2025)).
- **Western tropical Atlantic (Barbados):** Following the measurements from Cape Verde, HALO was transferred to Barbados to perform measurement flights over the western (sub-)tropical Atlantic until End of September 2024. During this part of the mission, the measurements were linked to ground-based measurements from the Barbados Cloud Observatory (BCO; Stevens, et al., 2016) on Barbados and to measurements onboard RV Meteor as part of BOWTIE. It also provided contrast in the convective and aerosol environment as compared to the Cape-Verde based measurements.
- **Extra-tropics (Oberpfaffenhofen, Germany):** After a small break, additional validation flights were performed out of Oberpfaffenhofen, the homebase of HALO, from 4 to 19 November 2024. This part of the campaign, was organized to coordinate with ground-based stations in Germany and Greece taking part in EarthCARE validation activities.

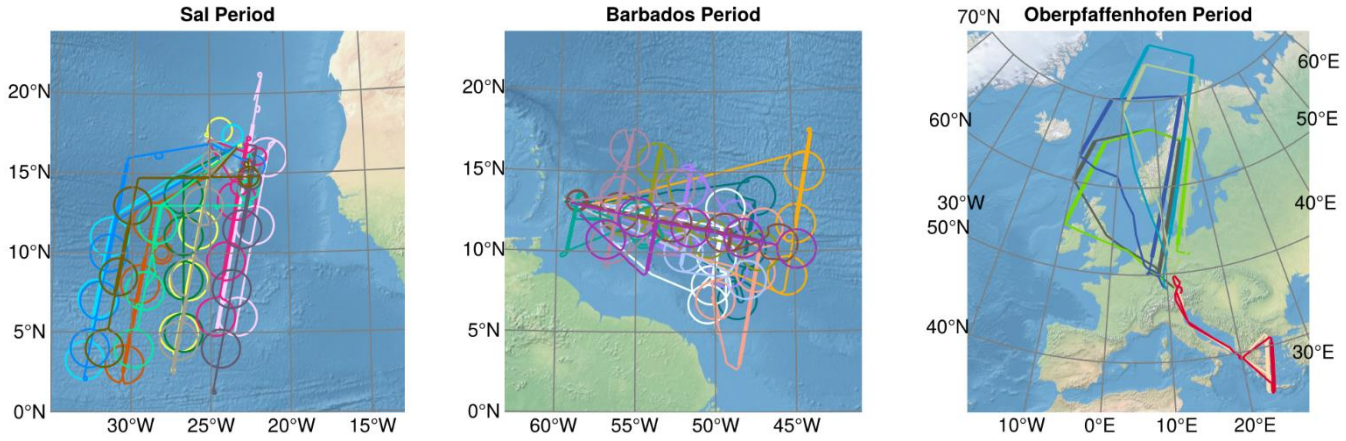

Figure 1: Flight tracks of the HALO research aircraft during the PERCUSION campaign out of Sal (left), Barbados (middle) and Oberpfaffenhofen (right). The straight thick lines indicate direct underpasses under the EarthCARE satellite. . The circles in the flights out of Sal and Barbados were performed to quantify meso-scale vertical motion.

The tropical flights constituted PERCUSION's contribution to ORCESTRA. Flights were anchored to EarthCARE underpass. This aided direct comparisons, but also put EarthCARE measurements in the center of scientific studies. For the tropical components of PERCUSION with flights out of Sal and Barbados, the EarthCARE track guided the position of the HALO flights, and thus helped avoid biassing the sampling of convection. The HALO flight plan, usually aligned with a descending (daytime) orbit of EarthCARE, but did not necessarily itself fly toward lower latitudes. The direct underpass was included in these straight flight legs captured different aerosol and cloud conditions and facilitated coordination with other measurements platforms (see e.g., Stevens et al, 2026 for coordination during ORCESTRA). For comparability of the EarthCARE and HALO measurements, we generally measured along the EarthCARE track for 10 minutes before and after coincidence. In addition to the straight flight legs on the EarthCARE tracks we included circles in the flight plan to investigate vertical motions (Bony and Stevens, 2019). Flights during ORCESTRA were conducted during daytime. Considering an EarthCARE equator crossing time around 14:00 local time, this results in an underpass time around 14:30-17:30 UTC (see Table 5). Information on flight plans, measurement situation and performance of each flight can be found at https://orcestra-campaign.org/operation/halo.html. The third part of PERCUSION, out of Oberpfaffenhofen, focused solely on EarthCARE validation. Flights were either planned at higher latitudes to capture continental conditions, cirrus clouds, and frontal cloud systems, and night-time conditions, or they were planned to measure in Mediterranean conditions with flights over the Greek ground-stations in Antikythera and Thessaloniki. During the northern flights we were sometimes able to underly EarthCARE twice on one flight. The time of the closest coincidence with EarthCARE was at around 15:00 and 17:00 UTC. In all the flights we included overpasses over ground-stations whenever possible.

In addition to our primary goal of validating EarthCARE, our efforts also address the validation of measurements and algorithms from NASA's PACE (Plankton, Aerosol, Cloud, Ocean Ecosystem) mission. To this end, we conducted four dedicated flights in the PACE swath during the campaign phase over the tropical western Atlantic. Furthermore, in preparation

for EarthCARE, we performed a series of underflights with the same payload under NASA's mission constellations CALIPSO and Cloudsat. Together with the measurements for EarthCARE validation, these underflights offer the opportunity to bridge some of the gaps arising from the two missions, such as those concerning wavelength dependence and sensitivities. Both topics will be addressed in the appendices of this manuscript.

3.4. Meeting EarthCARE

The validation of satellite data by airborne measurements benefits from the coincidence of the airborne and the spaceborne sensor footprints, as this is the easiest way to ensure that the airborne systems and the satellite systems are sampling the same airmasses. Table 5 summarizes information on co-location of HALO with EarthCARE during PERCUSION. Because PERCUSION took place early after the launch of EarthCARE, the satellite was still in a drifting phase, with periodic maneuvers, which made planning underflights more challenging. To account for this the flight path of HALO was adapted just before or partly even during the flight to benefit from the latest predictions. This worked well and we managed to capture EarthCARE with a cross-track distance of less than 500 m except for the two first flights, where we had a distance of about 1000 m. The ground footprint of the CPR is 750 m, while that of ATLID is 15 m, so that even with very good coincidence small scale differences from spatial sampling at the point of temporal collocation are to be expected. Differences will of course grow with increasing temporal dislocation, even as HALO flies along EarthCARE's track, something that needs to be considered.

In addition to the detailed information on the coincident point with EarthCARE, Table 3 also includes information on the scene that was targeted for comparison on the individual days. The table shows that all target scenes that have been identified as important (Section 2.2) for a full validation were captured during PERCUSION. Even a snow case was covered during one of the extra-tropical flights.

Table 5: Detailed information about EarthCARE underpasses including date of the flight, HALO base, underflown EarthCARE orbit, start time and end time on EarthCARE track (UTC), best match time (UTC), distance and location (lon/lat), and scene targeted for comparison.

Date	Base	Orbit	Time on EC track	Best match	Match dist.	Lon. °E	Lat. °N	Target Scenes
11 Aug.	Sal	01162E	15:22:37 – 16:09:11	15:52:02.743	996 m	-26.5562	17.1985	CC, CMA
13 Aug.	Sal	01193E	15:32:50 – 17:13:34	15:40:00.326	1090 m	-22.3079	17.1985	MAT
16 Aug.	Sal	01240E	16:03:18 – 16:51:28	16:14:04.527	441 m	-32.1054	7.3831	CLS, CC
18 Aug.	Sal	01271E	15:30:00 – 16:28:00	16:04:07.527	336 m	-29.7063	6.7818	CLS, CC
22 Aug.	Sal	01333E	14:57:00 – 16:04:00	15:41:22.111	131 m	-23.1087	14.1737	DC, LSR

25 Aug.	Sal	01380E	15:40:00 – 16:35:00	16:11:49.766	84 m	-30.9127	12.8612	MAT
27 Aug.	Sal	01411E	15:57:00 – 16:17:00	16:01:17.237	249 m	-26.9773	4.8126	MAT, CLS
29 Aug.	Sal	01442E	15:34:00 – 16:12:00	15:51:57.580	185 m	-22.6153	13.2611	DC, LSR
31 Aug.	Sal	01473E	15:24:00 – 16:00:00	15:38:41.850	253 m	-22.6153	13.2611	MAT
3 Sept.	Sal	01520E	16:00:00 – 16:34:00	16:09:04.874	22 m	-30.8138	8.6363	DC, LSR
7 Sept.	Barbados	01583E	17:10:00 – 17:39:00	17:18:30.109	192 m	-47.9594	10.4881	CLS
9 Sept.	Barbados	01614E	16:28:00 – 17:19:00	17:05:43.005	419 m	-44.1018	15.7095	MLS, CMA
12 Sept.	Barbados		17:10:00 – 17:53:00	17:35:33.811	30 m	-52.0739	12.1760	CMA
14 Sept.	Barbados	01692E	17:13:24 – 17:38:21	17:25:38.715	427 m	-49.8648	9.8595	CMA
16 Sept.	Barbados	01723E	16:52:00 – 17:51:00	17:16:06.878	384 m	-47.9917	5.8568	CMA, MSC
19 Sept.	Barbados	01770E	17:28:50 – 18:04:40	17:43:56.788	31 m	-53.8761	14.5050	CC, CMA
21 Sept.	Barbados	01801E	17:19:20 – 17:47:00	17:33:48.109	340 m	-51.7980	11.0166	CMA
23 Sept.	Barbados	01832E	17:14:00 – 17:24:00	17:22:33.535	330 m	-48.9818	11.1494	CC
24 Sept.	Barbados	01848E	17:48:00 – 18:17:40	18:03:00.027	298 m	-59.0219	11.7467	CC
26 Sept.	Barbados	01879E	17:20:40 – 18:21:00	17:51:55.041	291 m	-56.0327	13.5465	CLS, CMA
28 Sept.	Barbados	01910E	17:31:06 – 17:54:38	17:42:05.368	345 m	-53.9846	10.4329	CC, CMA
5 Nov.	Oberpf.	02499D	11:57:23 – 13:59:4	13:55:33.786	446 m	15.9275	64.3926	CC
		02500 D	15:26:03 – 16:07:26	15:28:00.709	475 m	-6.9707	64.7040	MSC, MAT
7 Nov.	Oberpf.	02530D	12:02:00 – 13:46:22	13:44:34.029	302 m	18.8376	64.6444	CLS, MSC
		02531D	15:16:19 – 16:48:19	15:17:02.613	309 m	-4.0945	64.9118	CC, MSC
10 Nov.	Oberpf.	02576D	12:15:04 13:02:30	12:48:48.217	226 m	23.0967	36.9121	CMA, CC
12 Nov.	Oberpf.	02608C/D	11:10:00 14:04:50	14:01:15.588	246 m	18.6452	69.3839	CC
		02609C/D	15:17:43 16:21:25	15:34:07.741	397 m	-5.7937	68.1341	CLS, SML
14 Nov.	Oberpf.	02639C/D	11:04:09 14:01:47	13:49:39.396	242 m	25.1685	72.3513	MLS, MSC

		02640C/D	14:47:13 15:38:00	15:22:16.125	296 m	1.7593	72.1700	CC
16 Nov	Oberpf.	02670C/D	11:47:09 13:58:49	13:39:50.884	329 m	23.8375	69.2438	DC, LSC
		02671C/D	14:52:16 15:36:22	15:11:40.927	426 m	3.9543	71.8482	CC, CMA
19 Nov.	Oberpf.	02716D	12:10:12 12:52:47	12:46:04.513	27 m	23.5290	35.8059	MAT, CMA

4. PERCUSION's potential for EarthCARE Validation

In the following we give examples of how HALO's measurements are being used for the validation of the EarthCARE data products. The examples are limited to individual EarthCARE overpasses to illustrate the direct comparability of the measurements. Future studies will present the results of the actual validation studies, including cross validation and statistical validation.

3.1. Atmospheric Lidar (ATLID)

WALES-ATLID comparison for Level 1 (L1) data

The lidar system WALES is an airborne water vapor differential absorption and high spectral resolution lidar (HSRL) developed and built at DLR (Wirth et al., 2009). It measures the water vapor field along the flight track from cruise altitude to ground with four wavelengths around 935 nm, and the extinction using the HSRL technique at 532 nm deploying an iodine filter. In addition, it is equipped with polarization sensitive measurements. The raw data resolution is 0.2 s, corresponding to about 44 m horizontal sampling for a typical aircraft speed of 220 m/s and 15 m in height. The processed data is typically provided horizontally integrated over 1 s (≈ 220 m) for the aerosol and cloud measurements and over 25 s for the water vapor data. To demonstrate the potential of WALES to validate ATLID-L1b (EarthCARE ATLID NOM Level 1B) and L2 (EarthCARE ATLID EBD Level 2A) optical properties derived by the A-PRO algorithm (Donovan et al., 2024), we focus on a research flight out of Sal on 13 August 2024, to compare ATLID aerosol measurements and products for orbit 01162. In this case a Saharan dust plume was mapped by both lidars which had been transported to the open ocean. Looking at the time-height cross section of the unpolarized backscatter coefficient (WALES) and unpolarized attenuated backscatter coefficient (ATLID) in Figure 2 we can identify an aerosol layer up to about 4 to 5 km altitude. Besides this aerosol layer, signatures of low clouds from about 0.5 km to about 2 km altitude are visible in the measurements of both systems (marked by the black out-of-scale color). In addition, enhanced backscattering at around 15 km altitude can be seen in the ATLID measurements, this layer is missed by the WALES measurements due to the lower flight altitude of HALO of about 11 km.

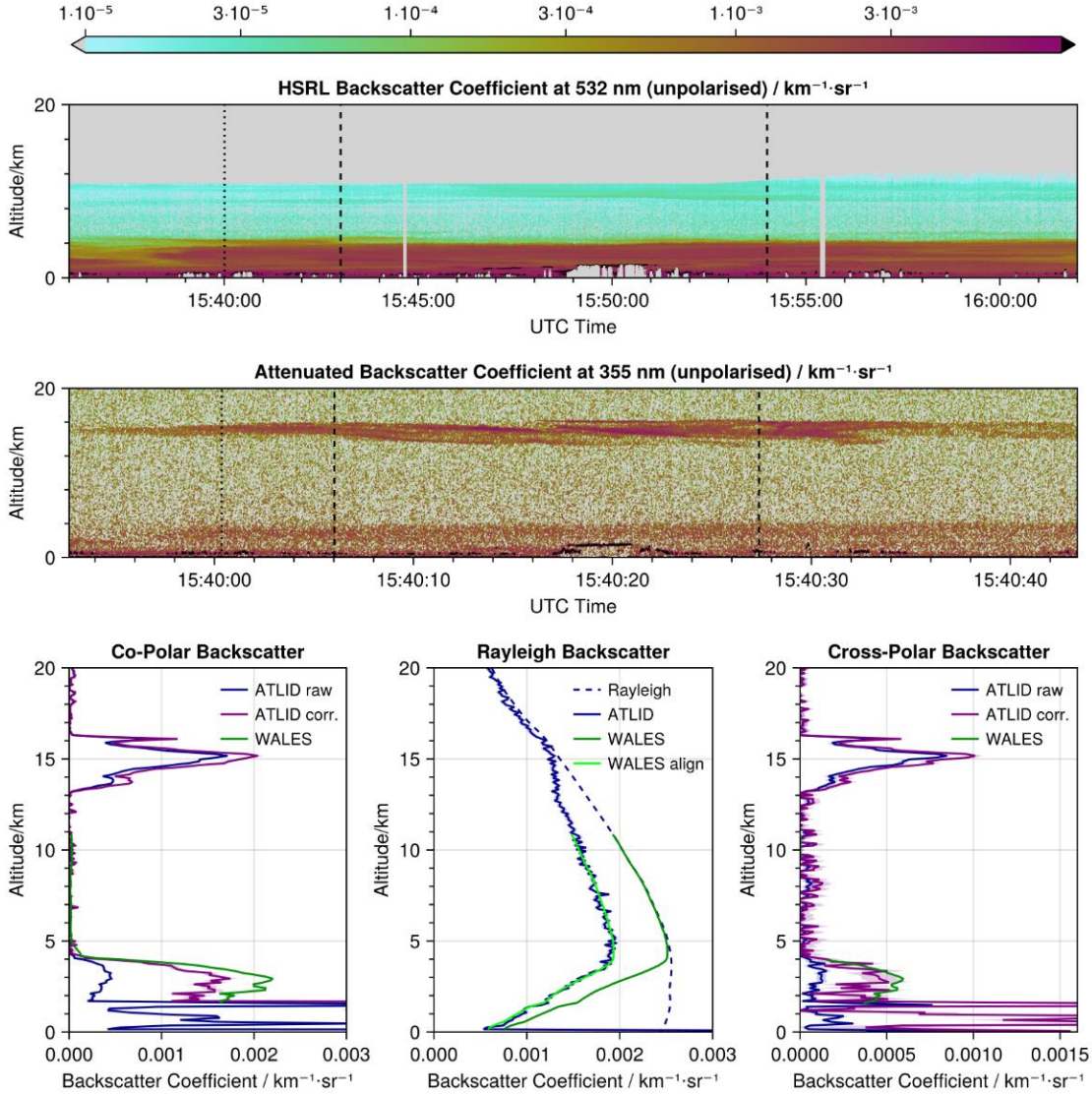

Figure 2: Comparison of the WALES HSRL Backscatter Coefficient at 532 nm (upper panel) and ATLID Attenuated Backscatter Coefficient at 355 nm (lower panel) for an underflight performed on 13 August 2024 out of Cape Verde. The dotted line shows the position of closest match. The dashed vertical lines mark the 150 km length region for the comparison of the co-polar backscatter profile, Rayleigh backscatter profile and cross-polar backscatter profile. The left lower panel shows the mean profiles of the backscatter coefficient for co-polar polarization for WALES (green) and for ATLID without extinction correction (blue) and in with extinction correction (purple). The middle lower panel shows the Rayleigh backscatter from ATLID (solid blue line), the expected pure Rayleigh backscatter signal calculated from an atmospheric density profile (dashed blue line) and the pure Rayleigh signal at 355 nm with additional aerosol extinction derived from the WALES measurements (dark green line). The light green line is aligned to the ATLID profile at the uppermost point of the WALES profile. The right lower panel shows the mean profiles of the backscatter coefficient for cross-polar polarization for WALES (green) and for ATLID without extinction correction (blue) and with extinction correction (purple). Semi-transparent bands around each profile indicate the one sigma statistical error as provided with the data products.

To validate ATLID L1 products, we compare the profiles of the measured Mie backscatter coefficient, Rayleigh backscatter coefficient, and Cross-polar backscatter coefficient as contained in the ESA ATL_NOM_1B product. We here use baseline

BA, where *baseline* means product version in ESA's nomenclature. As the measurement situation is stable (Figure 2) for comparisons of the co-polar backscatter coefficient, Rayleigh backscatter coefficient and cross-polar backscatter coefficient a region of 150 km length with homogenous backscatter close to the overpass point is selected to increase the signal-to-noise ratio (SNR) of ATLID data for the comparison. Directly around the overpass point the aerosol distribution is very structured which could lead to larger representativeness errors when averaged. For the comparison of L1 data we have to take into account, that ATLID and WALES are operated at different wavelengths, i.e. 355 nm and 532 nm, respectively. The backscatter coefficient for co-polar polarization for WALES and for ATLID is shown without extinction correction as contained in the L1 product and with correction for aerosol and molecular extinction by dividing the co-polar signal by the Rayleigh signal (HSRL method, purple line). The WALES profile shown is fully corrected for extinction. For evaluating the ATLID Rayleigh backscatter coefficient, we take into account the expected pure Rayleigh backscatter signal calculated from an atmospheric density profile contained within the L1 data and this pure Rayleigh signal at 355 nm with additional aerosol extinction derived from the WALES measurements. We aligned this to the ATLID profile at the uppermost point of the WALES profile, because there is considerable extinction from an above cirrus cloud not represented in the WALES measurements. If the aerosol extinction derived from WALES at 532 nm is the same as at 355 nm this light green profile should follow the signal from the ATLID Rayleigh channel closely, which is actually the case here. The benefit of the general same measurement technique allows to address issues like cross-talk and background corrections. For the current baseline version (BA) of ATLID L1 data we can confirm a general good quality of the ATLID Mie and Rayleigh backscatter coefficient.

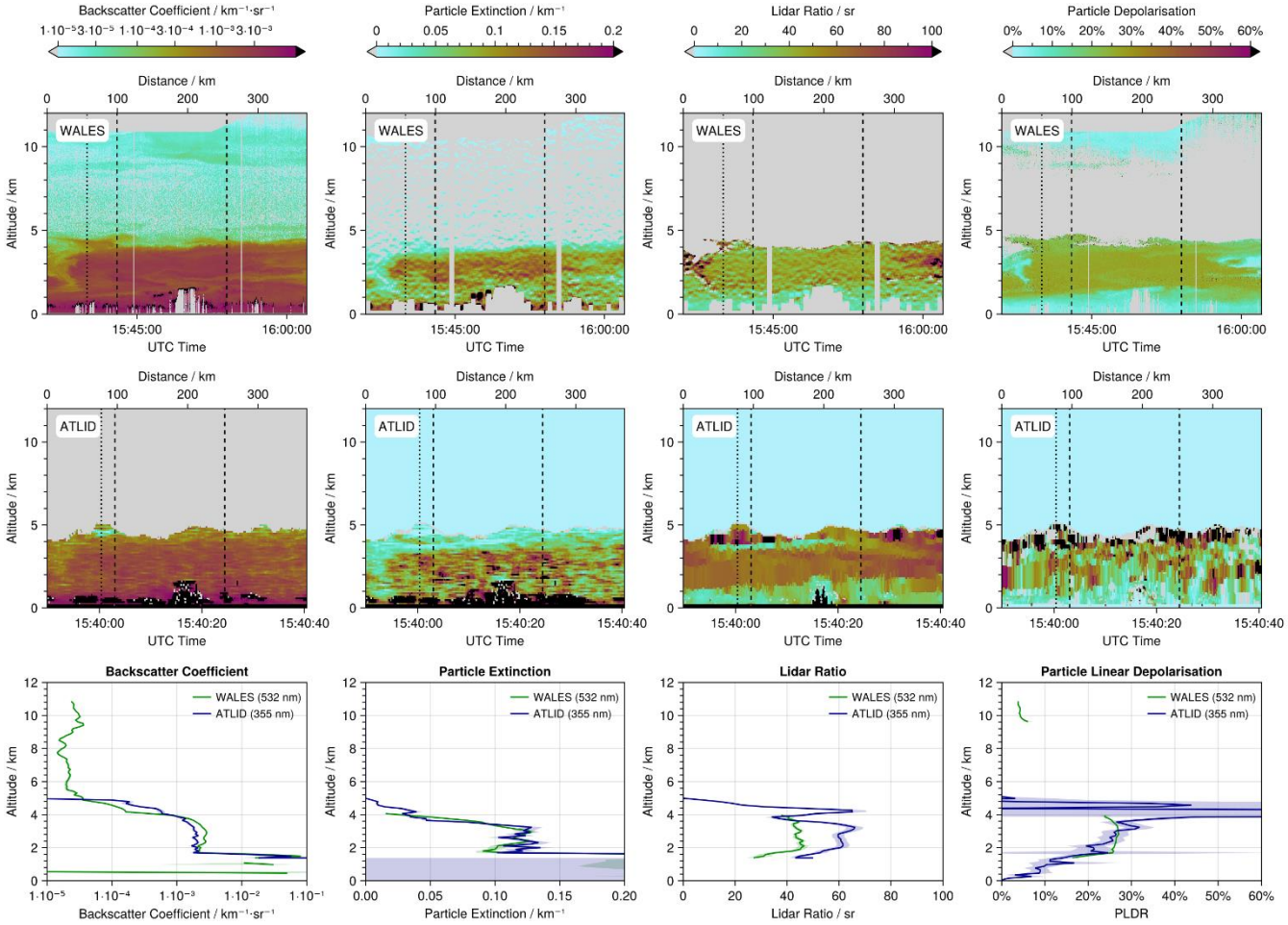

Figure 3: Time-height cross-section of the WALES optical properties (upper panel), and the ATLID optical properties (mid panel), and the profile comparisons (lower panel) of the backscatter coefficient (left), extinction coefficient (middle left), the lidar ratio (middle right), and the particle linear depolarization ratio (right) during the EarthCARE underpass on the 13 August 2013. The profiles are averaged within ±50 km around the EarthCARE overpass, indicated by the left and right vertical lines in the time-height cross-sections. Semi-transparent bands around each profile indicate the one sigma statistical error as provided with the data products.

WALES-ATLID comparison for Level 2 (L2) optical properties

After assessing the performance of the L1b data for this day, we investigate the quality of the ATLID L2a products of the cloud and aerosol profile processor (A-PRO) (Donovan et al., 2024), including the A-AER aerosol product, and the A-EBD extinction, backscatter, and depolarization product (A-EBD), the A-TC target classification product, and the A-ICE ice microphysical estimation product. For the example shown in Figure 2 we present the comparisons of WALES optical properties and A-EBD products, i.e., the extinction coefficient, the backscatter coefficient, the lidar ratio and the particle linear

depolarization ratio (Figure 3). For the validation analysis we use the latest available baseline version BA. Again, we have to consider a possible wavelength dependence. Former studies (e.g. Groß et al., 2011) confirm, that Saharan dust and marine aerosol layers do not show a wavelength dependence between 355 nm and 532 nm for the backscatter coefficient, extinction coefficient, and for the lidar ratio. For the particle linear depolarization ratio of Saharan dust, a small wavelength dependence between 355 nm and 532 nm is expected but well characterized (Freudenthaler et al., 2009; Groß et al., 2011; Groß et al., 2015; Groß et al., 2025; Burton et al., 2016; Haarig et al., 2022). Early comparisons between HALO measurements and ATLID L2 optical properties have identified an error in the layer specification for EarthCARE A-EBD algorithms, resulting in overly coarse layering. This problem could be solved before data have been made publicly available and are no issue anymore in the current baseline. Our comparisons confirm the good quality of the A-PRO products in the current baseline version in general. However, some differences between the WALES and ATLID data of the different products are visible. While the particle extinction coefficient shows agreement within the uncertainty range, significant differences occur for the values of the lidar ratio in the height range between about 1-4 km. The lidar ratio retrieved from ATLID data is about 60 sr while the corresponding data derived from WALES measurements is about 45 sr. This difference might result from the differences in the derived backscatter coefficient. The discrepancies might result from a wrong target classification and thus a wrong a priori information in the optimal estimate retrieval to derive A-EBD products, or a too strong weight on the a priori information. Investigations about this issue are ongoing. In addition, for the example shown, significant noise on the depolarization values is observed. Furthermore, especially the depolarization ratio shows a strange behavior at the upper edge of the aerosol layer leading to high, unphysical values.

WALES-ATLID comparison for L2 layer properties

Besides the L2 optical properties we use the WALES measurements for a comparison with the ATLID Target Classification (EarthCARE ATLID TC Level 2A) and the ATLID cloud top height (EarthCARE ATLID CTH Level 2A) (Wandinger et al., 2023) (baseline BA). An example comparison is shown for the HALO underflight on the 16 August 2024 southwest of Cabo Verde (orbit 01240E). This flight was selected as it captures a wide range of cloud and aerosol conditions typical of the tropical atmosphere. The flight objective aimed at a south-north transect across the ITCZ, including a flight leg of about 700 km (50 minutes) flown along the predicted EarthCARE ground track, extending from the ITCZ centre toward its northern edge. Figure 4a shows a time-altitude cross section of the backscatter ratio (BSR), which is the ratio of the total (aerosol + molecule) to the molecular backscatter signal, measured with the WALES instrument with the EarthCARE underpass at 16:14 UTC. The BSR measurements reveals several cloud and aerosol features that are captured in this flight section. At the highest altitudes (10-13 km) frequently large BSR values indicate a widespread field of ice clouds. This ice cloud field has the largest vertical extent near the underpass and is more patchy and thinner toward the northern part of the transect. At lower altitudes (1–3 km), smaller-scale regions of large BSR values are detected which are associated with stratocumulus and cumulus clouds. Additionally in the lowermost 6 km, an extended layer characterized by moderate BSR values (BSR between 2-6) is observed which indicates an aerosol layer. Notably, this aerosol layer appears thicker and more continuous in the northern segment (distance > 400 km)

of the flight leg. In the southern part, it appears as two separated layers: an elevated layer around 5 km altitude and another layer within the lowest 2 km of the atmosphere Threshold-based detection algorithms are commonly applied to determine atmospheric targets from lidar observations such as clouds and aerosols (Groß et al., 2013; Marinou et al., 2019). In this example, however, the focus is exclusively on the validation of EarthCARE cloud products. In particular, we focus on cloud macro-physical properties from the target classification product (A-TC), providing information on the vertical distribution of clouds and the cloud top height product (A-CTH). The A-TC classification itself applies height-dependent thresholds to ATLID backscatter and depolarization together with information on the tropopause height to distinguish between atmospheric target (Irbah et al., 2023). For the validation, cloud pixels and the altitude of the uppermost cloud layer are independently determined from the WALES backscatter ratio (BSR) data using a height-dependent threshold-based algorithm similar to approaches used in previous studies (e.g., Groß et al., 2014; Urbanek et al., 2017; Gutleben et al., 2019; Dekoutsidis et al., 2024). The specific implementation of this algorithm is described in detail in Krüger et al. (2026, in preparation) and is applied exclusively to the WALES observations.

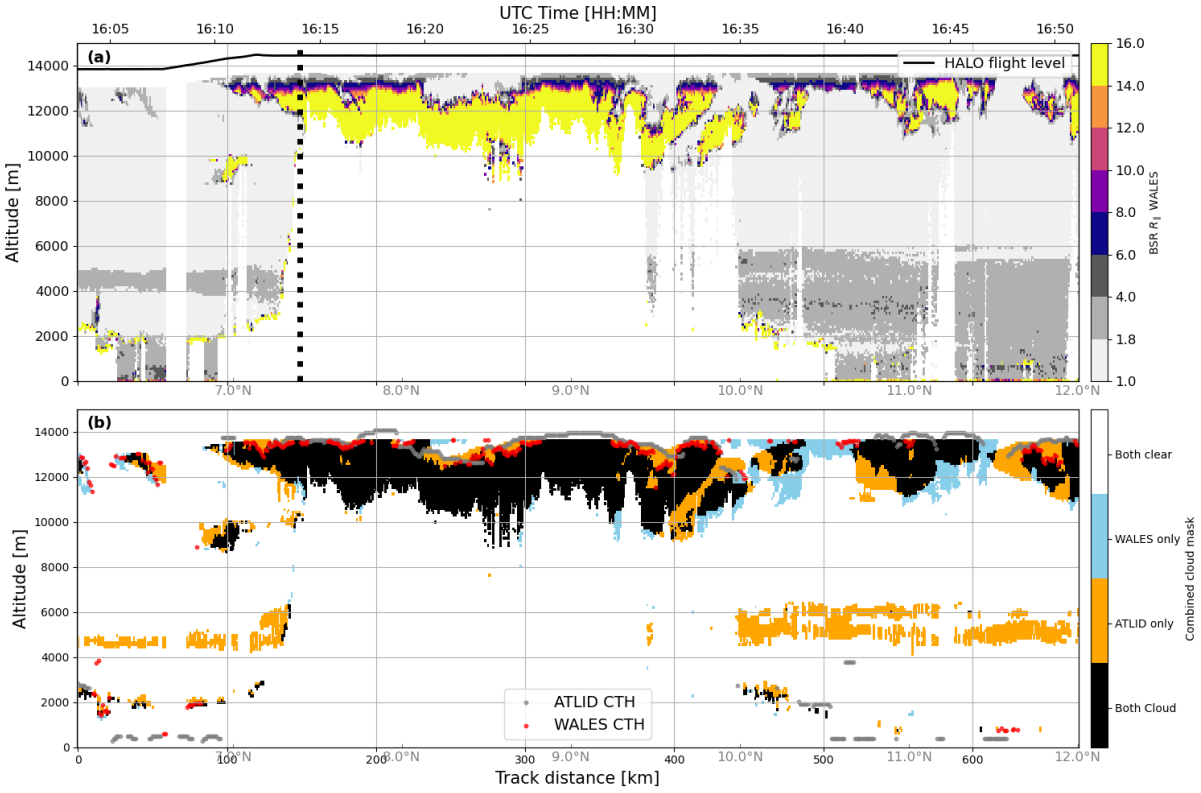

Figure 4: Distance–altitude cross sections for the HALO flight on 16 August 2024 showing (a) the backscatter ratio measured with the WALES HSRL, along with the flight altitude of the HALO aircraft (black solid line) and the EarthCARE underpass track (thick black dashed line). Panel (b) shows the combined cloud mask derived from the WALES BSR data and the collocated EarthCARE Level-2 target classification product (A-TC). Black shading indicates cloud pixels detected by both WALES and A-TC, while blue and orange colors represent cloud pixels identified exclusively by WALES or A-TC, respectively. White denotes regions with no cloud detection by either product. The red markers indicate the cloud top height derived from the WALES backscatter ratio, while

the gray markers represent the cloud top height from the A-CTH product. Note that cloud tops from WALES are displayed only when they could be unambiguously identified (e.g., when the cloud top was sufficiently far from the HALO aircraft), while A-CTH reports a cloud top for these cases.

Figure 4b shows the cross section of the combined cloud mask from WALES BSR and A-TC to directly compare both products along the coordinated EarthCARE underflight. The black shaded areas indicate a strong agreement in the vertical distribution of cloud pixels in both cloud masks, especially for high-altitude cirrus clouds and for the cumulus cloud formations at altitudes between 1 and 3 km. Interestingly, A-TC-only pixels (orange), associated with both cirrus and cumulus clouds, indicate comparatively thicker vertical clouds. Cirrus clouds in particular are more horizontally spread, and thus less patchy in the A-TC cloud mask. This might lead to vertically thicker cirrus clouds in the A-TC, corresponding to the elevated cloud tops (red line) of the A-CTH product. Furthermore, it is noted that the A-TC-only mask shows a coherent cloud structure at an altitude between 4 and 6 km, which corresponds exactly to the upper part of the aerosol layer (Figure 4a) suggesting a misclassification of cloud and aerosols in this scene. The BSR measurements illustrate that the WALES-BSR dataset can be reliably used to determine macro-physical cloud properties (e.g., vertical distribution, horizontal and vertical extent, and cloud top information), and to validate the ATLID level 2 relevant products. The case study presented indicates that the A-TC product reliably represents all cloud features observed by WALES (extended high-altitude clouds and low-altitude clouds). There are indications that the cloud pixels in A-TC, especially ice clouds, are too large horizontally and vertically, which could be due to "bad layering" in the product algorithms. There are also indications that the cloud tops of the independent A-CTH product are higher than those derived from WALES and, in some cases, inconsistent with the cloud mask of A-TC.

3.2. Cloud Profiling Radar (CPR)

The radar onboard HALO is a high-power (30 kW peak) magnetron-based MIRA35 cloud radar at 35.2 GHz manufactured from METEK. It has been thoroughly characterized and calibrated (Ewald et al., 2019). With a repetition rate of 7.5 kHz, the minimum detectable signal at 10 km (1s avg) is around -42 dBZ and thus at least 6 dB higher compared to CPR. Including effects of platform motion and natural spectral width, the effective sensitivity is around -34 dBZ. The vertical resolution of the MIRA measurements is significantly finer (30 m vs 500 m), and the horizontal resolution is twice as high (200 m vs 500 m) compared to CPR. Due to the lower frequency (35 vs 94 GHz), the gaseous and hydrometeor attenuation is also considerably lower for MIRA observations.

Figure 5 shows the comparisons between space- and airborne measurements of the radar reflectivity (Figure 5a, b) and Doppler velocity (Figure 5c, d) performed on the 18 August 2024 (orbit 01271E). The observations were carried out in the Tropical

Atlantic roughly 1500 km south-east from Cape Verde above a convective region within the ITCZ.

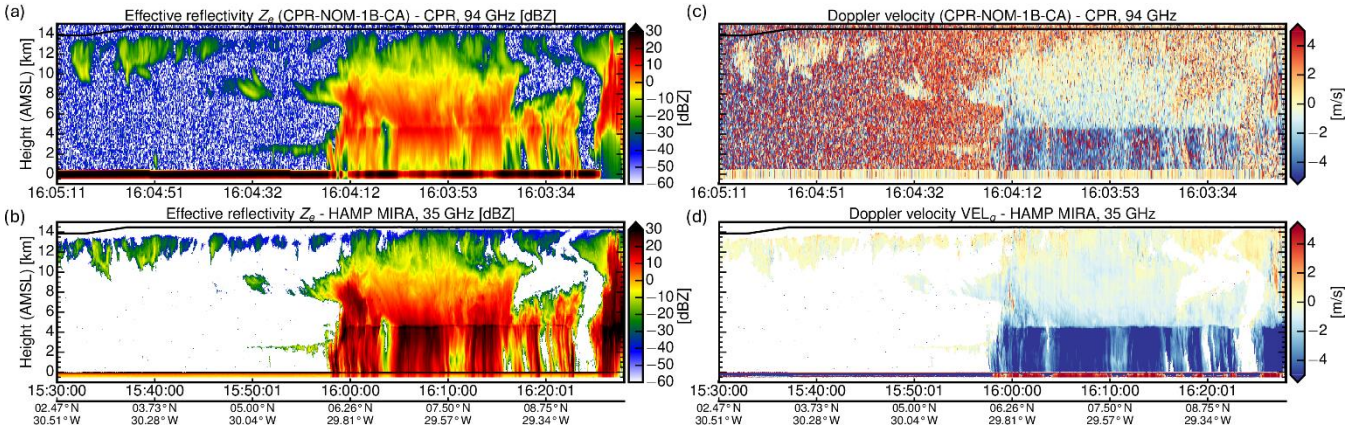

Figure 5: Comparison of (a) CPR and (b) MIRA radar reflectivity and of the Doppler velocity from (c) CPR and (d) MIRA for a HALO underpass of EarthCARE performed on 18 August 2024.

Between the measured radar reflectivity from CPR (Figure 5a) and MIRA (Figure 5b), the coarser resolution and slightly lower sensitivity of CPR is most apparent for the thin cirrus at cloud top. Moreover, the different Mie scattering regime and the different absorption by hydrometeors stands out in the rain region below the melting layer. As this measurement was acquired during the commissioning phase of EarthCARE, the redundant signal processing unit (SPU-A) of CPR was used which exhibited a drift in the Doppler velocity background signal (see clear-sky regions in Figure 5c), biasing low echo cloud regions which disappeared after switch to the operational signal processing unit (SPU-B) on 4 December 2024. This increased the noise in Doppler measurements (Figure 5c) and caused the rainbow-like pattern in the clear-sky region. Figure 6 compares the mean profiles of radar reflectivity (Figure 6a, NOM-1B-CA) and Doppler velocity (Figure 6b, CD-2A-AC) in absolute numbers. In the cloud top region between 6-10 km with negligible gaseous and hydrometeor attenuation and predominant Rayleigh scattering, the radar reflectivity bias was initially quite negative (-3.8 dB) for the early processing baseline BA. The bias improved to -1.6 dB for baseline CA until it was resolved for baseline CB. For the level 2 Doppler velocity product CD-2A, the antenna miss-pointing correction by Puigdomènech Treserras et al. (2025) successful removed any velocity biases. Below an altitude of 6 km, the radar reflectivity mainly differs due to the differential hydrometeor attenuation between 35 GHz and 94 GHz. The difference in the mean Doppler velocity can be explained by Mie scattering at 94 GHz of larger and faster falling rain droplets, underrepresenting their faster velocity component in the mean Doppler velocity.

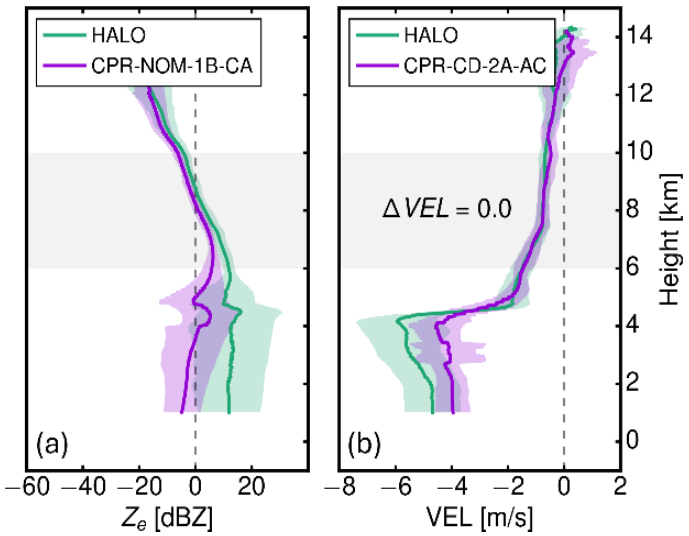

Figure 6 Comparison of mean observed profiles between HALO and EarthCARE (a) Radar reflecitivtyL1 product CPR-NOM-1B-CA and (b) L2 product CPR-CD-2A-AC for the underflight shown in Figure 5.

3.3. Multi Spectral Imager (MSI)

4.3.1 Comparison specMACS-MSI

The specMACS consists of two hyperspectral line cameras (Ewald et al., 2016) covering the visible and near-infrared (VNIR, 400 - 1000 nm) and the short-wave infrared (SWIR, 1000 - 2500 nm), as well as four two-dimensional polarization resolving RGB cameras (Weber et al., 2024), providing an across-track field of view of about 220°. The VNIR and SWIR measurements during the 33 EarthCARE underflights of the PERCUSION campaign allow a direct comparison of the measured reflected radiances to the ones measured by the four MSI channels with center wavelengths at 670 nm and 865 nm in the VNIR and 1650 nm and 2210 nm in the SWIR, respectively. An appropriate validation can only be performed for the nadir pixel of the two cameras at the exact time of the overflight, since all other pixels are observed under different viewing angles.

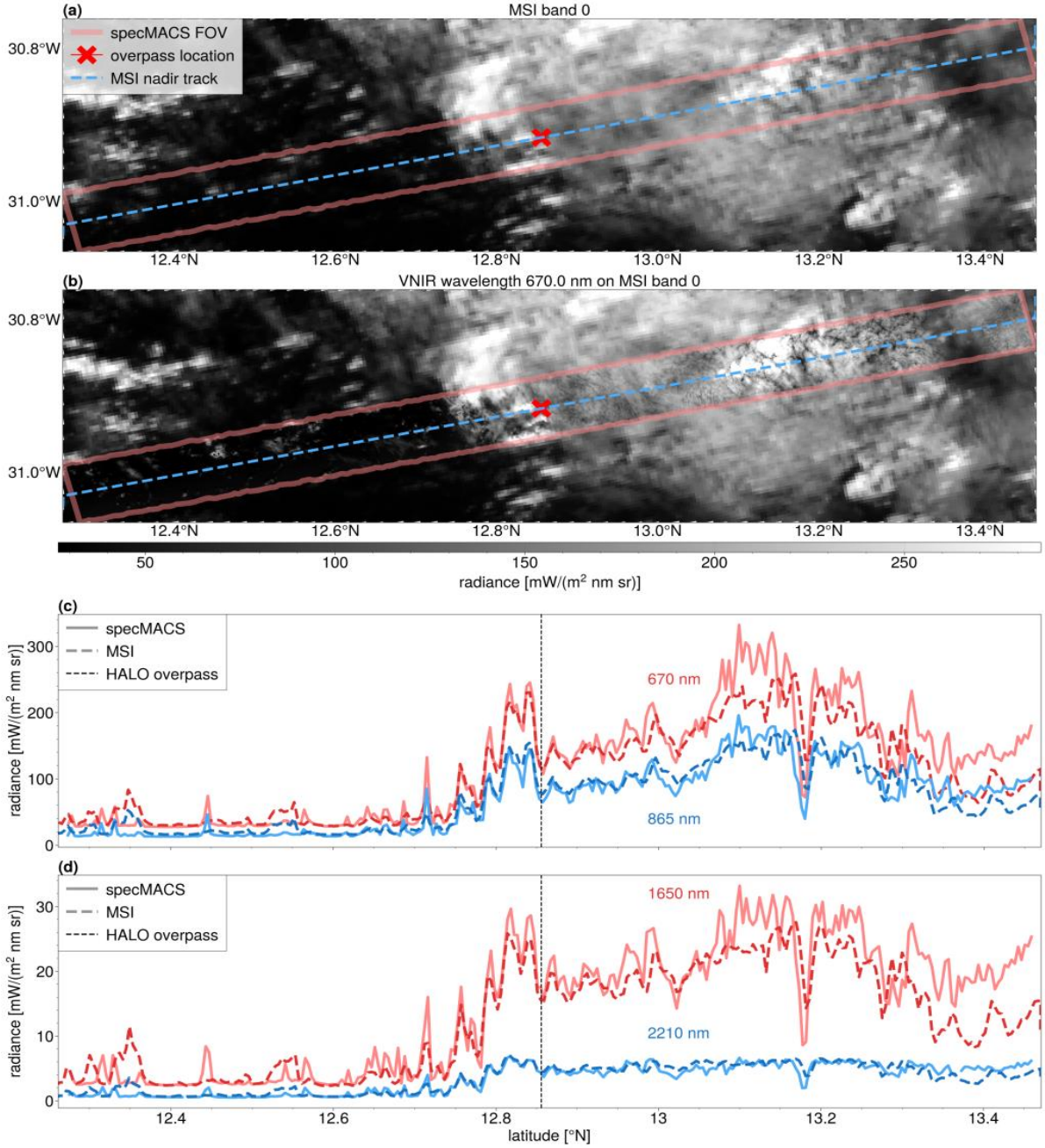

Figure 7: Comparison of specMACS to MSI on 25 August 2024. In a, the measurement of the MSI band 0 is shown for the considered measurement region. In panel b, the corresponding specMACS measurement at a wavelength of 670 nm is overlayed. Panels c and d show comparisons of the measured nadir pixel radiances of the two VNIR bands (panel c) and SWIR bands (panel d) with respect to the latitude. The dotted line is the overpass best match.

In the following, we consider the overflight on 25 August 2025 (01380E) with a horizontal distance of about 84 m over the northern tropical Atlantic. In Figure 7, we show the 10 minutes around the overflight time for specMACS, corresponding to

approximately 19 s for MSI to cover the same field of view (FOV). Figure 7a shows the radiances as seen by the visible channel of MSI. In red, the specMACS field of view is shown, while the blue dashed line depicts the nadir pixel track of the MSI band 0. The cross denotes the location of the overpass. The corresponding measurements of the 670 nm channel of the VNIR are overlayed on the MSI measurements in Figure 7b. Clearly, one can see the same cloud field, with a significantly higher spatial resolution of specMACS (typically around 15 m for the VNIR and less than 40 m for the SWIR at a distance of 10 km to the cloud compared to about 500 m of MSI). In Figure 7c, we show a quantitative comparison of the nadir pixels of the MSI bands 0 and 1 to the nadir pixels of the corresponding center wavelength channels of the VNIR averaged to the spatial extent of the individual MSI nadir pixels. Figure 7d shows the same for the two SWIR channels. The black dashed line depicts the time of the overpass with good agreement between specMACS and MSI around it. For the 670nm channel, we find a mean bias and standard deviation of -1.28 ± 6.93%, and hence slightly smaller radiances of MSI compared to specMACS, and a correlation coefficient of 0.93 for the entire segment. For the 865 nm band, we get 1.95 ± 7.64% for the mean bias and 0.93 for the correlation coefficient. For the SWIR channels, we find similar biases of -2.20 ± 8.51% for 1650 nm and 1.94 ± 8.63% for the 2210 nm channel, however, they show slightly larger standard deviations. For the correlation coefficients we derive 0.92 for both channels underscoring the good agreement between the two instruments taking into account that we include time differences of around 10 minutes between the specMACS and MSI measurements. Good agreement between the two instruments is particularly also observed for clear-sky pixels over the ocean where time shifts between MSI and specMACS are less important. For clouds further away from the overpass time, shifts in extrema and systematic differences can be identified which are possibly due to cloud movement and development over time. Despite those smaller differences, there is a clear potential for the validation of MSI radiances with the airborne measurements of the two hyperspectral cameras of specMACS. Furthermore, L2 products, such as cloud top height, cloud phase and cloud effective radius, could be compared in the future. In particular, one could also take into account the products of the polarization resolving cameras, which use a stereographic algorithm to determine cloud geometry (Kölling et al., 2019; Volkmer et al., 2024), a new approach to derive the cloud phase (Weber et al., 2025) and measurements of the cloud bow to derive the effective radius without being subject to 3-D effects which strongly affect classical bi-spectral methods (Pörtge et al., 2023).

4.3.2 Comparison VELOX-MSI

The thermal-infrared (TIR) imager VELOX (Video airbornE Longwave Observations within siX channels; (Schäfer, et al., 2022) onboard HALO measured two-dimensional fields of brightness temperature in two broadband and four narrow-band spectral channels with a horizontal resolution of 10 m for a typical HALO flight altitude of 10 km. The three VELOX channels centered at 8.7 µm, 10.7 µm and 12.0 µm were selected to match the MSI channels TIR-1 (8.8 µm), TIR-2 (10.8 µm) and TIR-3 (12.0 µm). Thus, VELOX measurements allow nighttime validation of MSI. During the PERCUSION campaign, several HALO flights were performed at high latitudes during twilight and night illumination conditions. On 16 November 2024, the HALO-EarthCARE underpass took place over the Norwegian Sea, where an air mass of Arctic origin was sampled. A variety of cloud structures was captured by MSI channel TIR-2 (Figure 8a). For a ±2.5-minute sequence around the underpass, a

pushbroom-like image was constructed based on 10.7 µm VELOX images and mapped on top of the MSI image (Figure 8b). In general, MSI and VELOX show similar features in the cloud structure. However, due to the dynamics of the scene a point-by-point validation is challenging and limited to the underpass location. To allow for a fair comparison, the high spatial resolution of the VELOX measurement (12.5 m) was scaled to the MSI resolution (500 m) and spatially matched. To compensate for the dynamics of the scene, swath averages were calculated for both measurements (Figure 8c). A linear fit was applied yielding a coefficient of determination R^2 of 0.7. The mean bias for the swath averages of MSI and VELOX brightness temperatures was found to be about 0.15 K. Reflecting the variation of clouds in the scene, the swath standard deviations are equally large for both instruments. While both platforms are moving on different time scales, the spatial distance from the underpass is a common metric for quantifying the comparability. This metric ranges between 0 km and 35 km for the ±2.5-minute VELOX sequence and is used as a color-code in Figure 8c. Directly at the underpass the swath averages show a very good agreement (light blue markers). With increasing distance, there are mostly distinct brightness temperature differences (dark blue markers) of up to 9 K. However, the cloud movement depends on the local wind pattern, which was analyzed based on the auxiliary meteorological database (X-MET products, baseline AA) and the ATLID feature mask (baseline BA) to identify high and low cloud layers. In this case, higher (~ 9 km) and lower clouds (~ 2 km) experienced a southward shift caused by northerly winds and wind speeds of about 8 m s^{-1} and 17 m s^{-1}, respectively. For a 2.5-minute distance to the underpass this translates to a spatial displacement of about 1.2 km (~ 2-3 MSI pixels) for higher clouds and 2.6 km (~ 5-6 MSI pixels) for lower clouds. Nevertheless, based on the swath averages a comparison of MSI and VELOX shows a reasonable agreement. Further cases in other temperature regimes and during daytime need to be analyzed to extend the potential of the MSI-VELOX validation.

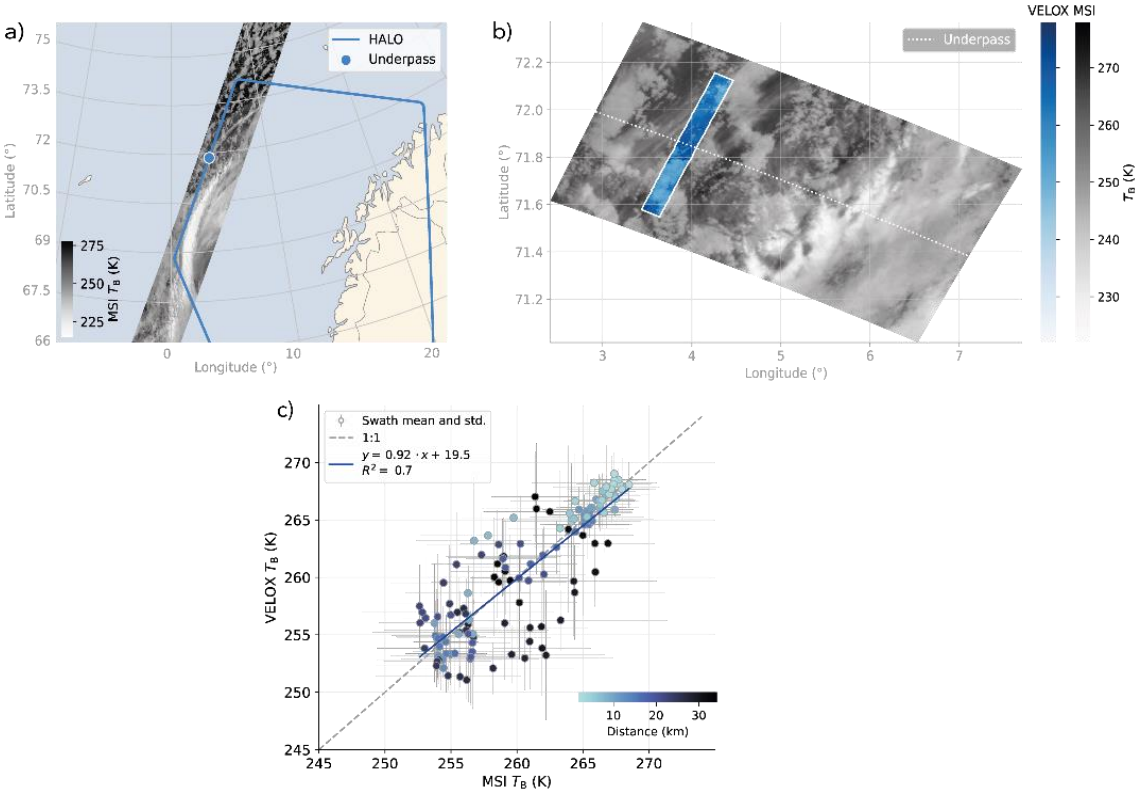

Figure 8: MSI-VELOX brightness temperature T_B comparison for the research flight on 16 November 2024. a) Map showing the HALO flight track and MSI T_B at 10.8 µm (TIR-2) for orbit 02671 frame C of baseline BA, the underpass location is marked. b) VELOX (10.7 µm) ±2.5-minute pushbroom image around the underpass mapped on top of the MSI T_B section. c) Comparison of MSI and VELOX swath T_B averages and standard deviations with a linear fit. Data points are colored by their spatial distance to the underpass location.

3.4. BroadBand Radiometer (BBR)

For the same flight section analyzed for the VELOX-MSI comparison in Section 4.3 the BBR L2 product BMA_FLX_2B (baseline AB) was evaluated by measurements on HALO. Due to the absence of solar radiation at these high latitudes the focus is on the thermal infrared irradiance derived from BBR measured radiances. On HALO, broadband upward thermal-infrared irradiance was measured with the Broadband AirCrAft RaDiometer Instrumentation system (BACARDI; (Ehrlich et al., 2023)). The uncertainties are mostly linked to the sensitivity calibration and are in the range of 45% (2 times the standard deviation confidence level). Thermal offset effects can be neglected for this case study, because HALO did not change altitude during the flight sections. Uncertainty estimates of BBR BMA_FLX_2B irradiances (baseline BA) are reported in the public release of the product, available by the end of 2025. However, for the section analyzed here, the BBR data status is of high to very high confidence. The comparisons of BBR and BACARDI for the 15 min flight section of the EarthCARE overpass are shown in Figure 9. The BACARDI raw data range significantly higher than BBR irradiances. This is due to the

emission/absorption of thermal infrared radiation by the atmosphere above the flight altitude of HALO (here about 12.5 km). As BBR measures broadband irradiance covering significant water vapor and ozone emission/absorption lines, this needs to be considered in the comparison to BACARDI. A correction based on radiative transfer simulations using the atmospheric properties from the AUX_MET_1D product was applied to the BACARDI data. The quality of the simulations was confirmed by comparing the downward thermal infrared irradiance that has additionally been derived from the simulations and was also measured by BACARDI. The flight section averages amount to 19 W m^{-2} (simulations) and 19 W m^{-2} (BACARDI) and show negligible differences. As shown in Figure 9 (blue line), the flight altitude correction of the BACARDI measurement shifts the airborne observations close to the BBR data. The mean upward irradiance of BACARDI was corrected from 199.3 Wm^{-2} to 192.8 Wm^{-2} matching the BBR product of 186.4 Wm^{-2} within the uncertainty range of BACARDI. While the average irradiances agree, some deviations of the variations in the time series are obvious. This likely results from the increasing time shift between EarthCARE and HALO observations and the different footprints of the BBR and BACARDI sensors. Depending on the reference altitude of the observed scene (e.g., cloud top altitude), the hemispheric integrating optical inlet of BACARDI covers a larger area and less variability than BBR. Further studies and different cloudy and cloud-free scenes are needed to explore these effects in detail.

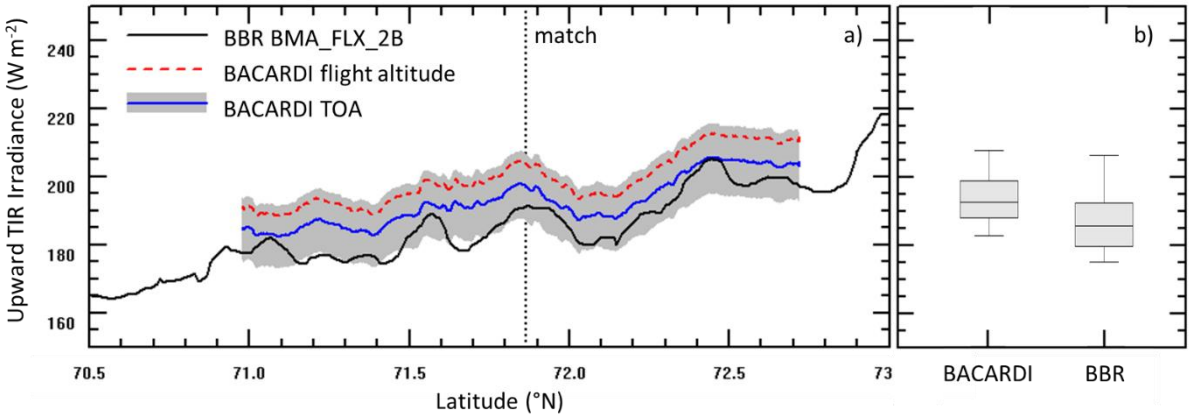

Figure 9: a) Time series (displayed as latitude) of upward thermal-IR irradiance measured by BACARDI and retrieved by BBR for 16 November 2024 (orbit 02671, frame C). Raw data and data corrected for flight altitude are displayed for BACARDI measurements. The box-wisker plot in b) show only corrected BACARDI data.

3.5. Synergy and radiative consistency

To evaluate the performance of the synergistic EarthCARE products (first data have been made publicly available Dec. 2025), we further developed independent synergistic lidar-radar retrievals (Delanoë and Hogan, 2008) to derive height-resolved information of ice (Cazenave et al., 2019), and mixed-phase and supercooled liquid (Aubry et al., 2024) cloud microphysical properties. Measurements of the infrared (IR) emissivity (Delanoë and Hogan, 2008) or of the reflected solar radiation (Ewald et al., 2021) help to constrain the retrieved microphysical properties. Additionally, one can also use the measured radiative

quantities to check the retrieved microphysical properties for consistency or to control the assumptions. The microphysical properties are retrieved using an optimal estimation framework. Next, the reflected solar radiation is simulated using the radiative transfer code (libRadtran; Mayer and Kylling, 2005) and compared with the measured solar radiation measured onboard the HALO aircraft. The same can be done using measurements onboard the EarthCARE satellite.

Similarly, we can perform radiative closure for aerosol scenes, using information on microphysical properties from data bases (e.g. (Gasteiger et al., 2011; Gasteiger and Wiegner, 2018)) or from in-situ measurements (e.g. Weinzierl et al., 2011). To validate the EarthCARE products, we leverage a combination of airborne and satellite-based observations collected during PERCUSION. As an example, we performed simulations for the EarthCARE underpass on 22 August 2024, focusing on cloud free aerosol conditions. High-resolution lidar measurements of aerosol and water vapor profiles and aerosol optical properties derived from the hybrid end-to-end aerosol classification model for EarthCARE (HETEAC; Wandinger et al., 2023) were used as input for radiative transfer simulations. The calculated radiances were compared to measured radiances from specMACS. More precisely, broadband solar radiances were computed in the wavelength range 500–900 nm, matching the visible-near infrared (VNIR) spectral coverage of specMACS (Ewald et al., 2016). The simulations were carried out for the flight altitude and for each ~1 km nadir point along a 10 km track centred around the EarthCARE and the HALO meeting point for cloud-free (in terms of cloud) conditions. The closure revealed a good agreement with measured radiances, with a mean absolute 10 km along track difference between simulated and measured radiances of -0.07 $Wm^{-2}sr^{-1}$ (Figure 10) which corresponds to a relative difference of -0.9%. For a demonstration of how radiative consistency serves for validation and to advances the understanding of the radiative impact of the atmospheric constituents, the closure was performed with airborne observations. Once the full EarthCARE dataset will be released, this study is extended using EarthCARE top-of-atmosphere (TOA) radiances and fluxes from the BBR, and including EarthCARE aerosol profiles and other atmospheric input parameters. The study does also account for new and more realistic optical properties for non-spherical dust particles.

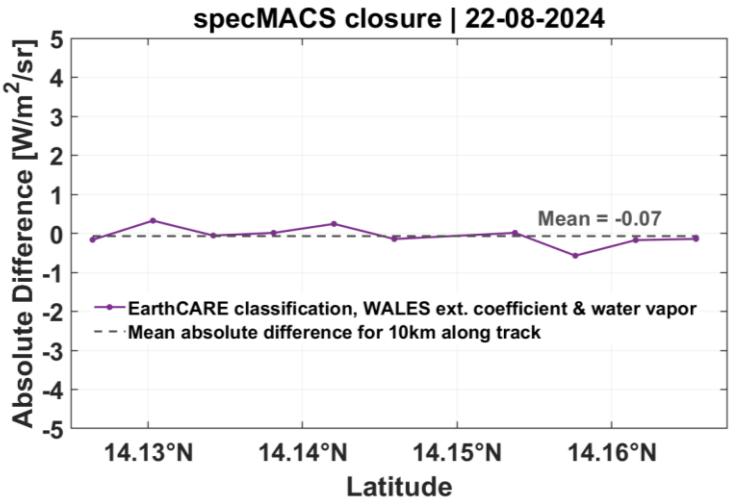

Figure 10: Differences between simulated and observed broadband SW radiances along the 10 km along track on the 22nd of August. The dashed lines denote the mean 10 km along track differences.

5. Summary and Conclusion

Airborne measurements with an EarthCARE-like payload on the German research aircraft HALO were performed during the PERCUSION campaign. In addition to its scientific objectives PERCUSION was designed to contribute to the validation of EarthCARE data products. During PERCUSION HALO performed measurements using similar instruments deployed in a similar fashion, i.e., with respect to viewing angle, as for EarthCARE. The HALO measurements are well characterized and calibrated and have finer sensitivity and resolution than those made by EarthCARE (Stevens et al., 2019; Groß and Ewald, 2018), thus making them well suited for validation studies. To assess higher level EarthCARE data products, we developed independent algorithms and analysis tools to take advantage of the full suite of HALO measurements.

PERCUSION took place during the EarthCARE commissioning phase and started with the first flight on the day EarthCARE instruments were set to operational mode. Thirty flights, with 33 direct underpasses were flown out of three locations —Cape Verde, Barbados, and Southern Germany — in summer and fall 2024 to sample a wide variety of different aerosol and cloud situations and meteorological conditions. With this intense measurement period and a sophisticated flight planning, we captured all of the target scenes that have been defined as important for EarthCARE (Hall, 2025) to provide data that allows a comprehensive validation on EarthCARE data products..

We highlight the applicability of the PERCUSION measurements for EarthCARE validation through selected examples. These show the applicability of PERCUSION's measurements to the validation of each of the four sensors aboard EarthCARE, and highlight some early issues for more detailed studies.

A conclusive statement about the validation is difficult because the processing of the EarthCARE and HALO data is updated as we gain a better understanding of the measurements. Hence validation is a moving target. For instance, at the very beginning of the EarthCARE mission, PERCUSION measurements helped identify cross-talk effects, background suppression or calibration uncertainties that improved the first release of EarthCARE data products. of ATLID L1b data. It also helped to identify artefacts resulting from bugs in the layer assignment in the algorithm for the ATLID L2a optical products. Airborne radar data from PECUSION measurements helped to identify an offset of the CPR compared to MIRA measurements, and motivated a new calibration of the radar, which led to a much-improved data quality. With the help of the airborne data these problems could be solved quickly and the products publicly available have been updated.

Several issues remain. For instance, a misclassification of aerosol and cloud scenes that arises from horizontal variability might have a significant impact on follow-on studies and data exploitation. The passive sensors onboard HALO while suggesting a generally good agreement with the MSI, appear biased relative to the BBR. Detailed studies are ongoing and being updated as data products are preprocesses based on findings from PERCUSION's and other validation studies.

In addition to the validation of EarthCARE data products, PERCUSION measurements are also being used for the validation of the measurements and algorithms of NASA's PACE (Plankton, Aerosol, Cloud, ocean Ecosystem) mission. We performed four dedicated flights within the swath of the PACE mission, three of them along the satellite track (Appendix A). Furthermore, with the EarthCARE-like payload on HALO, and especially with the combination of the lidar and the radar, we performed a large number of underflights under the CALIPSO and Cloudsat mission during past campaigns, as well as under the EarthCARE mission, and thus provide underflights under both satellite constellation and mission with combined lidar and radar payload to bridge the gap from CALIPSO/Cloudsat to EarthCARE (Appendix B).

Data availability

The EarthCARE Level-1 products and Level-2 products used in this study are publicly accessible from the ESA Earth Online gateway. The WALES measurements are available from Zenodo with DOI 10.5281/zenodo.15527242 for the Cape Verde period (Wirth 2025a), DOI 10.5281/zenodo.17153149 for the Barbados period (Wirth and Groß, 2025a), 10.5281/zenodo.17153625 for the Germany period (Wirth and Groß, 2025b). specMACS data are made available under request. HALO Radar data are available from Zenodo with DOI 10.5281/zenodo.17910007 (Ewald and Groß, 2025), BACARDI data are available from Zenodo with DOI 10.5281/zenodo.18999496 (Luebke et al., 2026), the SMART measurements are available via the HALO-Database and the VELOX data will be made available via the IPFS ORCESTRA data browser. In addition, MIRA cloud radar data and the WALES lidar data for the A-Train underflights with HALO listed in Table B1 are available via Zenodo with DOI 10.5281/zenodo.19317830 (Ewald, 2026) and DOI 10.5281/zenodo.19318124 (Ewald and Wirth, 2026), respectively.

Author contribution

SG developed the outline of the paper and wrote the first draft with contributions of FE, BS, MW, GD, AE, DK, KK, SR, LV. SG developed the strategy for EarthCARE validation within PERCUSION together with BS, JW, FE, and MR. JvB, LH, RK, MPS provided the essential coordination of PERCUSION and EarthCARE. AL, BM, MW helped with the overall design of the validation campaign activities and flight planning, and are responsible for validation sub-activities within PERCUSION. All authors read the paper and discussed the findings.

Acknowledgements

We thank the flight Experiment Facility of DLR for preparing and performing the measurement flights and providing the HALO meteorological measurements. We acknowledge the contribution of Kevin Wolf, Michael Schäfer and Patrizia Schoch for operating SMART and VELOX during the flights and processing the data, of Anna Weber, Tobias Zinner, Veronika Pörtge, Zekican Demiralay and Anja Stallmach for the operation of specMACS and the data processing, of Sabrina Zechlau for performing flights with the WALES system, and Tanja Bodenbach for operating the WALES during flights and providing technical support, of Christian Heske, Felix Ament, and Janina Boemeke for operating the MIRA during specific flights.

Financial support

The PERCUSION campaign was partly funded by the DFG (Deutsche Forschungsgemeinschaft) within the Priority Program (Schwerpunktprogramm) SPP 1294 'Atmospheric and Earth System Research with HALO' (project grant no. 316646266**)**, and by internal funding of the Max-Planck Institute for Meteorology in Hamburg, and the Institute of Atmospheric Physics of the German Aerospace Center (DLR). This study was supported by ESA under the campaign activity 'EarthCARE: Give Airborne with Radar, Lidar –HALO EC- TOOC and Home-Base' under ESA Contract No. 4000145500/24/NL/SC, by the Obs3RvE (Optimising 3D RT Earthcare product using geostationary observations and AI) project under Contract No. 4000147848/25/I/AG, and by the EarthCARE Data Innovation and Science Cluster (DISC) under Contract No. 4000144997/24/I-NS. The analysis of this project has further received funding from Horizon Europe programme under Grant Agreement No 101137680 via project CERTAINTY (Cloud-aERosol inTeractions & their impActs IN The earth sYstem), and by the PANGEA4CalVal project (Grant Agreement 101079201) funded by the European Union. Furthermore, the traveling to the field campaign has been supported by the DLR internal project MABAK (Innovative Methoden zur Analyse und Bewertung von Veränderungen der Atmosphäre und des Klimasystems). This research has furthermore been supported by the DFG under Grant Nos 502197012, 502188551.

Competing interests

At least one of the (co-)authors is a member of the editorial board of Atmospheric Measurement Techniques.

References

Amiridis, V., Marinou, E., Hostetler, C., Koopman, R., Cecil, D. J., Moisseev, D., . . . co-authors.: Best practices for the validation of Aerosol, Cloud, and Precipitation Profiles (ACPPV). (Zenodo, Hrsg.) doi:https://doi.org/10.5281/zenodo.15025627, 2025.

Aubry, C., Delanoe, J., Groß, S., Ewald, F., Tridon, F., Jourdan, O., and Mioche, G.: Lidar-radar synergistic method to retrieve ice, supercooled water and mixed-phase cloud properties. *Atmos. Meas. Tech., 17*, 3863--3881. doi:https://doi.org/10.5194/amt-17-3863-2024, 2024.

Barker, H. W., Korolev, A. V., Hudak, D. R., Strapp, J. W., Strawbridge, K. B., and Wolde, M.: A comparison between CloudSat and aircraft data for a multilayer, mixed phase cloud system during the Canadian CloudSat-CALIPSO Validation Project. *Journal of Geophysical Research, 113*(D00A16). doi:doi:10.1029/2008JD009971, 2008.

Bedka, K. M., Nehrir, A. R., Kavaya, M., Barton-Grimley, R., Beaubien, M., Carroll, B., . . . Skofronick-Jackson, G.: Airborne lidar observations of wind, water vapor, and aerosol profiles during the NASA Aeolus calibration and validation

(Cal/Val) test flight campaign. *Atmos. Meas. Tech.s, 14*, 4305--4334. doi:https://doi.org/10.5194/amt-14-4305-2021, 2021.

Bony, S., and Stevens, B.: Measuring Area-Averaged Vertical Motions with Dropsondes. *Journal of Atmospheric Science, 76*(3), 767--783. doi:https://doi.org/10.1175/JAS-D-18-0141.1, 2019.

Burton, S. P., Ferrare, R. A., Vaughan, M. A., Omar, A. H., Rogers, R. R., Hostetler, C. A., and Hair, J. W.: Aerosol classification from airborne HSRL and comparisons with the CALIPSO vertical feature mask. *Atmos. Meas. Tech., 6*, 1397--1412. doi:https://doi.org/10.5194/amt-6-1397-2013, 2013.

Burton, S. P., Hair, J. W., Kahnert, M., Ferrare, R. A., Hostetler, C. A., Cook, A. L., . . . Rogers, R. R.: Observations of the spectral dependence of linear particle depolarization ratio of aerosols using NASA Langley airborne High Spectral Resolution Lidar. *Atmos. Chem. Phys., 15*, 13453--13473. doi:https://doi.org/10.5194/acp-15-13453-2015, 2016.

Cazenave, Q., Ceccaldi, M., Delanoe, J., Pelon, J., Groß, S., and Heymsfield, A.: Evolution of DARDAR-CLOUD ice cloud retrievals: new parameters and impacts on the retrieved microphysical properties. *Atmos. Meas. Tech., 12*, 2819--2835. doi:https://doi.org/10.5194/amt-12-2819-2019, 2019.

Dekoutsidis, G., Wirth, M., and Groß, S.: The effects of warm-air intrusions in the high Arctic on cirrus clouds, Atmos. Chem. Phys., 24, 5971–5987, https://doi.org/10.5194/acp-24-5971-2024, 2024.

Delanoë, J., and Hogan, R.: A variational scheme for retrieving ice cloud properties from combined radar, lidar, and infrared radiometer. *Journal of Geophysical Research, 113*(7). doi:10.1029/2007JD009000, 2008.

Delanoe, J., Ament, F., Ceccaldi, M., Groß, S., Hagen, M., Hirsch, L., . . . Vinson, J.-P.: Airborne EarthCare Preparation, Calibration and Validation Tandem System. *EarthCARE Workshop.* Tokyo. doi:https://elib.dlr.de/90952/, 2014.

Delanoë, J., Groß, S., Ewald, F., Cazenave, Q., Pelon, J., Marinou, E., and Ibrah, A.: *EPATAN project.* ESA. doi:https://doi.org/10.5270/ESA-a346352, 2020.

Donovan, D. P., Zadelhoff, G.-J. v., and Wang, P.: The EarthCARE lidar cloud and aerosol profile processor (A-PRO): the A-AER, A-EBD, A-TC, and A-ICE products. *Atmos. Meas. Tech., 17*, 5301--5340. doi:https://doi.org/10.5194/amt-17-5301-2024, 2024.

Ehrlich, A., Zöger, M., Giez, A., Nenakhov, V., Mallaun, C., Maser, R., . . . Wendisch, M.: A new airborne broadband radiometer system and an efficient method to correct dynamic thermal offsets. *Atmos. Meas. Tech., 16*, 1563--1581. doi:https://doi.org/10.5194/amt-16-1563-2023, 2023.

Eisinger, M., Marnas, F., Wallace, K., Kubota, T., Tomiyama, N., Ohno, Y., . . . Bernaerts, D.: The EarthCARE mission: science data processing chain overview. *Atmos. Meas. Tech., 17*(2), 839--862. doi:https://doi.org/10.5194/amt-17-839-2024, 2024-

Emde, C., Buras-Schnell, R., Kylling, A., Mayer, B., Gasteiger, J., Hamann, U., . . . Bugliaro, L.: The libRadtran software package for radiative transfer calculations (version 2.0.1). *Geoscientific Model Development, 9*, 1647-1672. doi:10.5194/gmd-9-1647-2016, 2016.

ESA: *Validation Needs*. Von https://earth.esa.int/eogateway/missions/earthcare/data/calibration-validation/validation-needs, 2024.

ESA: *Introducing EarthCARE's Data, Innovation and Science Cluster*. Von https://earth.esa.int/eogateway/news/introducing-earthcare-s-data-innovation-and-science-cluster, 2024.

Ewald, F.: MIRA cloud radar data from A-Train underflights with HALO (Radar reflectivity) [Data set]. Zenodo, https://doi.org/10.5281/zenodo.19317830, 2026.

Ewald, F., and Wirth, M: WALES lidar data from A-Train underflights with HALO (Backscatter coefficient) [Data set]. Zenodo. https://doi.org/10.5281/zenodo.19318124, 2026.

Ewald, F., Groß, S., Hagen, M., Hirsch, L., Delanoe, J., and Bauer-Pfundstein, M.:. Calibration of a 35 GHz airborne cloud radar: lessons learned and intercomparisons with 94 GHz cloud radars. *Atmos. Meas. Tech.s, 12*, 1815-1839. doi:10.5194/amt-12-1815-2019, 2019.

Ewald, F., Groß, S., Wirth, M., Delanoe, J., Fox, S., and M. B.: Why we need radar, lidar, and solar radiance observations to constrain ice cloud microphysics. *Atmos. Meas. Tech.s, 14*(7). doi:https://doi.org/10.5194/amt-14-5029-2021, 2021.

Ewald, F., Kölling, T., Baumgartner, A., Zinner, T., and Mayer, B.: Design and characterization of specMACS, a multipurpose hyperspectral cloud and sky imager. *Atmos. Meas. Tech., 9*(5), 2015-2042. doi:10.5194/amt-9-2015-2016, 2016.

Fix, A., Amediek, A., Ehret, G., Groß, S., Kiemle, C., Reitebuch, O., and Wirth, M.:. On the Benefit of airborne emonstrators or space borne lidar missions. (I. -I. Optics, Hrsg.) *Proc. of SPIE, Vol. 10562*. doi:doi: 10.1117/12.2296197, 2016.

Floutsi, A. A., Rizos, K., Trapon, D., Engelmann, R., Althausen, D., Marinou, E., . . . Baars, H.: On the representativeness of the ground-based lidar observations for satellite calibration/validation – the example of the archipelago of Cabo Verde. *EGUsphere*. doi:https://doi.org/10.5194/egusphere-2025-4742, 2025.

Freudenthaler, V., Esselborn, M., Wiegner, M., Heese, B., Tesche, M., Ansmann, A., . . . Seefeldner, M.:. Depolarization ratio profiling at several wavelengths in pure Saharan dust during SAMUM 2006. *Tellus B: Chemical and Physical Meteorology, 61*(1), 165--179. doi:DOI: 10.1111/j.1600-0889.2008.00396.x, 2009.

Gasteiger, J., and Wiegner, M.: MOPSMAP v1.0: a versatile tool for the modeling of aerosol optical properties. *Geoscientific Model Development, 11*(7), 2739--2018. doi:https://doi.org/10.5194/gmd-11-2739-2018, 2018.

Gasteiger, J., Wiegner, M., Groß, S., Freudenthaler, V., Toledano, C., Tesche, M., and Kandler, K.: Modelling lidar-relevant optical properties of complex mineral dust aerosols. *Tellus B: Chemical and Physical Meteorology, 63*(4), 725--741. doi:https://doi.org/10.1111/j.1600-0889.2011.00559.x, 2011, 2011.

Getzewich, B. J., Vaughan, M. A., Hunt, W. H., Avery, M. A., Powell, K. A., Tackett, J. L., . . . Toth, T. D.: CALIPSO lidar calibration at 532 nm: version 4 daytime algorithm. *Atmos. Meas. Tech., 11*, 6309--6326. doi:https://doi.org/10.5194/amt-11-6309-2018, 2018.

Giez, A. Z., Mallaun, C., Nenakhov, V., Schimpf, M., Grad, C., Numberger, A., and Raynor, K.: Determination of the Measurement Errors for the HALO Basic Data System BAHAMAS by Means of Error Propagation. (D. Z.-u. Raumfahrt, Hrsg.) *DLR-Forschungsbericht*. doi:10.57676/5rdc-q708, 2023.

Gimmestad, G., Forrister, H., Grigas, T., and O'Dowd C.: Comparisons of aerosol backscatter using satellite and ground lidars: implications for calibrating and validating spaceborne lidar. *Sci Rep 7*, 42337, https://doi.org/10.1038/srep42337, 2017.

Gloeckner, H. M., Mieslinger, T., Robbins-Blanch, N., George, G., Kluft, L., Kölling, T., Bony, S., Windmiller, J., and Stevens, B.: BEACH: Barbados and Eastern Atlantic Combined High-altitude dropsonde datasets, Earth Syst. Sci. Data Discuss. [preprint], https://doi.org/10.5194/essd-2025-647, in review, 2025

Groß, S., and Ewald, F.: NARPEX project - Final Report. DLR. Von https://elib.dlr.de/216858/, 2018.

Groß, S., Esselborn, M., Weinzierl, B., Wirth, M., Fix, A., and Petzold, A.: Aerosol classification by airborne high spectral resolution lidar observations. *Atmospheric Chemistriy and Physics*, *13*, 2487–2505. doi:10.5194/acp-13-2487-2013, 2013.

Groß, S., Freudenthaler, V., Haarig, M., Ansmann, A., Toledano, C., Mateos, D., . . . Weinzierl, B.: Characterization of aerosol over the eastern Mediterranean by polarization-sensitive Raman lidar measurements during A-LIFE – aerosol type classification and type separation. *Atmos. Chem. Phys.*, *25*, 3191--3211. doi:https://doi.org/10.5194/acp-25-3191-2025, 2025.

Groß, S., Freudenthaler, V., Schepanski, K., Toledano, C., Schäfler, A., Ansmann, A., and Weinzierl, B.: Optical properties of long-range transported Saharan dust over Barbados as measured by dual-wavelength depolarization Raman lidar measurements. *Atmos. Chem. Phys.*, *15*, 11067--11080. doi:https://doi.org/10.5194/acp-15-11067-2015, 2015.

Groß, S., Freudenthaler, V., Wirth, M., and Weinzierl, B.: Towards an aerosol classification scheme for future EarthCARE lidar observations and implications for research needs. *Atmospheric Science Letter*, *16*, 77--82. doi:https://doi.org/10.1002/asl2.524, 2015.

Groß, S., Tesche, M., Freudenthaler, V., Toledano, C., Wiegner, M., Ansmann, A., . . . Seefeldner, M.:. Characterization of Saharan dust, marine aerosols and mixtures of biomass-burning aerosols and dust by means of multi-wavelength depolarization and Raman lidar measurements during SAMUM 2. *Tellus B: Chemical and Physical Meteorology*, *63*(4), 706--724. doi:https://doi.org/10.1111/j.1600-0889.2011.00556.x, 2011.

Groß, S., Wirth, M., Schäfler, A., Fix, A., Kaufmann, S., and Voigt, C.: Potential of airborne lidar measurements for cirrus cloud studies, Atmos. Meas. Tech., 7, 2745–2755, https://doi.org/10.5194/amt-7-2745-2014, 2014.Gutleben, M., Groß, S., and Wirth, M.: Cloud macro-physical properties in Saharan-dust-laden and dust-free North Atlantic trade wind regimes: a lidar case study. *Atmos. Chem. Phys.*, *19*, 10659-10673. doi:10.5194/acp-19-10659-2019, 2019

Gutleben, M., Groß, S., Heske, C., and Wirth, M.: Wintertime Saharan dust transport towards the Caribbean: an airborne lidar case study during EUREC4A. *Atmos. Chem. Phys.*, *22*, 7319--7330. doi:https://doi.org/10.5194/acp-22-7319-2022, 2022

Gutleben, M., Groß, S., Wirth, M., and Mayer, B.: Radiative effects of long-range-transported Saharan air layers as determined from airborne lidar measurements, Atmos. Chem. Phys., 20, 12313–12327, https://doi.org/10.5194/acp-20-12313-2020, 2020.

Gutleben, M., Groß, S., Wirth, M., Emde, C., and Mayer, B.: Impacts of water vapor on Saharan air layer radiative heating. *Geophysical Research Letters, 46*, 14854--14862. doi:https://doi.org/10.1029/2019GL085344, 2019.

Haarig, M., Ansmann, A., Engelmann, R., Baars, H., Toledano, C., Torres, B., . . . Wandinger, U.: First triple-wavelength lidar observations of depolarization and extinction-to-backscatter ratios of Saharan dust. *Atmos. Chem. Phys., 22*, 355--369. doi:https://doi.org/10.5194/acp-22-355-2022, 2022.

Hair, J. W., Hostetler, C. A., Ferrare, R. A., Cook, A. L., and Harper, D. B.:. The NASA Langley airborne high spectral resolution lidar for measurements of aerosols and clouds. *Reviewed and Revised Papers Presented at the 23rd International Laser Radar Conference* (S. 411--414). Tokyo: Tokyo Metropolitan University. https://laser-sensing.jp/ilrc23_CD1a2b3c/ILRC23/3P-5.pdf, 2006.

Hair, J. W., Hostetler, C. A., Cook, A. L., Harper, D. B., Ferrare, R. A., Mack, T. L., Welch, W., Izquierdo, L. R. and Hovis, F. E.: Airborne High Spectral Resolution Lidar for profiling aerosol optical properties, *Appl. Opt.* 47, 6734-6752 2008.

Hall, A.: *EarthCARE Validation – Level 2 Algorithm Developer Needs*, https://earth.esa.int/eogateway/documents/d/earth-online/earthcare-validation-l2-algorithm-developer-needs-table, 2005

Irbah, A., Delanoë, J., van Zadelhoff, G.-J., Donovan, D. P., Kollias, P., Puigdomènech Treserras, B., Mason, S., Hogan, R. J., and Tatarevic, A.: The classification of atmospheric hydrometeors and aerosols from the EarthCARE radar and lidar: the A-TC, C-TC and AC-TC products, *Atmos. Meas. Tech.*, 16, 2795–2820, https://doi.org/10.5194/amt-16-2795-2023 , 2023

IPCC: *Climate Change 2021 – The Physical Science Basis.* (I. P. (IPCC), Hrsg.) Cambridge University Press. doi:https://doi.org/10.1017/9781009157896, 2023.

Kacenelenbogen, M., Redemann, J., Vaughan, M. A., Omar, A. H., Russell, P. B., Burton, S., . . . Hostetler, C. A.: An evaluation of CALIOP/CALIPSO's aerosol-above-cloud detection and retrieval capability over North America. *Journal of Geophysical Research: Atmosphere, 119*, 230--244. doi:doi:10.1002/2013JD020178, 2014.

Kar, J., Vaughan, M. A., Lee, K.-P., Tackett, J. L., Avery, M. A., Garnier, A., . . . Winker, D. M.:. CALIPSO lidar calibration at 532 nm: version 4 nighttime algorithm. *Atmos. Meas. Tech., 11*, 1459--1479. doi:https://doi.org/10.5194/amt-11-1459-2018, 2018.

King, M. D., Menzel, W. P., Granz, P. S., Myers, J. S., Arnold, G. T., Gumley, L. E., . . . Osterwisch, F. G.: Airborne Scanning Spectrometer for Remote Sensing of Cloud, Aerosol, Water Vapor, and Surface Properties. *Journal of Atmospheric and Oceanic Technology, 13*(4), 777--794. doi:https://doi.org/10.1175/1520-0426(1996)013<0777:ASSFRS>2.0.CO;2, 1996.

Kölling, T., Zinner, T., and Mayer, B.:. Aircraft-based stereographic reconstruction of 3-D cloud geometry. *Atmospheric Measurements Techniques, 12*, 1155--1166. doi:https://doi.org/10.5194/amt-12-1155-2019, 2019.

Koopmann, R.:. *Scientific Validation Implementation Plan*, https://earth.esa.int/eogateway/documents/d/earth-online/earthcare-scientific-validation-implementation-plan, 2024

Krautstrunk, M., and Giez, A.: The Transition From FALCON to HALO Era Airborne Atmospheric Research. *Atmospheric Physics: Background-Methods-Trends*, 609--624, doi:https://doi.org/10.1007/978-3-642-30183-4_37https://doi.org/10.1007/978-3-642-30183-4_37, 2012.

Krüger, K., Groß, S., and Wirth, M.: Validation of cloud macrophysical properties from the ATLID L2a products A-TC, A-FM, A-CTH using airborne lidar observations during the HALO missions PERCUSION, ASCCI and NAWDIC, (to be submitted to AMT, 2026).

Langsdale, M., Verhoelst, T., Povey, A. et al.: The Challenges and Limitations of Validating Satellite-Derived Datasets Using Independent Measurements: Lessons Learned from Essential Climate Variables. *Surv Geophys*. https://doi.org/10.1007/s10712-025-09898-4, 2025.

Lemmerz, C., Lux, O., Witschas, B., Rahm, S., Marksteiner, U., Geiß, A., . . . Reitebuch, O.:. Airborne Doppler wind LIDAR technology demonstration for Aeolus: from pre-launch campaigns to mission performance validation. *Proc. SPIE 12777, International Conference on Space Optics — ICSO 2022, 1277707*. doi:https://doi.org/10.1117/12.2688591, 2023.

Luebke, A. E., Ehrlich, A., Wolf, K., Giez, A., Zöger, M., Mallaun, C., Nenakhov, V., Eirenschmalz, L., Pasternak, D., Rosenburg, S., Schäfer, M., Schoch, P., & Wendisch, M.: Broadband solar and thermal-infrared, upward and downward irradiance measured by BACARDI during the PERCUSION field campaign [Data set]. Zenodo. https://doi.org/10.5281/zenodo.18999496, 2026.

Lux, O., Lemmerz, C., Weiler, F., Marksteiner, U., Witschas, B., Rahm, S., . . . Reitebuch, O.: Airborne wind lidar observations over the North Atlantic in 2016 for the pre-launch validation of the satellite mission Aeolus. Atmos. Meas. Tech., 11, 3297--3322. doi:https://doi.org/10.5194/amt-11-3297-2018, 2018.

Lux, O., Lemmerz, C., Weiler, F., Marksteiner, U., Witschas, B., Rahm, S., . . . Reitebuch, O.: Retrieval improvements for the ALADIN Airborne Demonstrator in support of the Aeolus wind product validation. Atmos. Meas. Tech., 15, 1303--1331. doi:https://doi.org/10.5194/amt-15-1303-2022, 2022.

Marinou, E., Amiridis, V., Paschou, P., Tsekeri, A., Tsikoudi, I., and Voudouri, K.-A.: Across Mediterranean Experiment for the Cal/Val of the Earthcare Mission. IGARSS 2024 - 2024 IEEE International Geoscience and Remote Sensing Symposium. doi:10.1109/IGARSS53475.2024.10642456, 2024.

Marinou, E., Ewald, F., Gross, S., Wirth, M. S., Cazenave, Q., and Delanoe, J.: Aerosol-Cloud Target Classification in HALO Lidar/Radar Collocated Measurements. EPJ Web of Conferences, 237, 08002. doi:https://doi.org/10.1051/epjconf/202023708002, 2020.

Mayer, B., and Kylling, A.: Technical note: The libRadtran software package for radiative transfer calculations - description and examples of use. Atmos. Chem. Phys., 5, 1855--1877. doi:https://doi.org/10.5194/acp-5-1855-2005, 2005.

McGill, M. J., Vaughan, M. A., Trepte, C. R., Hart, W. D., Hlavka, D. L., Winker, D. M., and Kuehn, R.: Airborne validation of spatial properties measured by the CALIPSO lidar. Journal of Geophysical Research, 112(D20201). doi:doi:10.1029/2007JD008768, 2007.

Mech, M., Orlandi, E., Crewell, S., Ament, F., L., H., Hagen, M., . . . Stevens, B.: HAMP – the microwave package on the High Altitude and LOng range research aircraft (HALO). Atmos. Meas. Tech., 7(12), 4539-4553. doi:10.5194/amt-7-4539-2014, 2014.

Mieslinger, T., Stevens, B., Kölling, T., Brath, M., Wirth, M., and Buehler, S. A.: Optically thin clouds in the trades. Atmospheric Chemistry and Physics, 22(10), 6879–6898. https://doi.org/10.5194/acp-22-6879-2022, 2022.

Okamoto, H., Sato, K., Nishizawa, T., Jin, Y., Nakajima, T., Wang, M., Satoh, M., Suzuki, K., Roh, W., Yamauchi, A., Horie, H., Ohno, Y., Hagihara, Y., Ishimoto, H., Kudo, R., Kubota, T., and Tanaka, T.: JAXA Level2 algorithms for EarthCARE mission from single to four sensors: new perspective of cloud, aerosol, radiation and dynamics, Atmos. Meas. Tech. Discuss. [preprint], https://doi.org/10.5194/amt-2024-101, 2024.

Paffrath, U., Lemmerz, C., Reitebuch, O., Witschas, B., Nikolaus, I., and Freudenthaler, V.: The Airborne Demonstrator for the Direct-Detection Doppler Wind Lidar ALADIN on ADM-Aeolus. Part II: Simulations and Rayleigh Receiver Radiometric Performance. Journal of Atmospheric and Ocean Technology, 26, 2516--2530. doi:https://doi.org/10.1175/2009JTECHA1314.1, 2009.

Pörtge, V., Kölling, T., Weber, A., Volkmer, L., Emde, C., Zinner, T., . . . Mayer, B.:. High-spatial-resolution retrieval of cloud droplet size distribution from polarized observations of the cloudbow. Atmos. Meas. Tech., 6, 645--667. doi:https://doi.org/10.5194/amt-16-645-2023, 2023.

Puigdomènech Treserras, B., Kollias, P., Battaglia, A., Tanelli, S., and Nakatsuka, H.: EarthCARE's cloud profiling radar antenna pointing correction using surface Doppler measurements, Atmos. Meas. Tech., 18, 5607–5618, https://doi.org/10.5194/amt-18-5607-2025, 2025.

Reitebuch, O., Lemmerz, C., Nagel, E., Paffrath, U., Durand, Y., Endemann, M., . . . Chaloupy, M.: The Airborne Demonstrator for the Direct-Detection Doppler Wind Lidar ALADIN on ADM-Aeolus. Part I: Instrument Design and Comparison to Satellite Instrument. Journal of Atmospheric and Ocean Technology, 26, 2501--2515. doi:https://doi.org/10.1175/2009JTECHA1309.1, 2009.

Rogers, R. R., Ferrare, R. A., Liu, Z., Obland, M. D., Harper, D. B., Cook, A. L., . . . Winker, D. M.: Assessment of the CALIPSO Lidar 532 nm attenuated backscatter calibration using the NASA LaRC airborne High Spectral Resolution Lidar. 11, 1295--1311. doi:https://doi.org/10.5194/acp-11-1295-2011, 2011.

Rogers, R. R., Vaughan, M. A., Hostetler, C. A., Burton, S. P., Ferrare, R. A., Young, S. A., . . . Winker, D. M.:. Looking through the haze: evaluating the CALIPSO level 2 aerosol optical depth using airborne high spectral resolution lidar data. Atmos. Meas. Tech., 7, 4317--4340. doi:https://doi.org/10.5194/amt-7-4317-2014, 2014.

Röttenbacher, J., Ehrlich, A., Müller, H., Ewald, F., Luebke, A. E., Kirbus, B., . . . Wendisch, M.: Evaluating the representation of Arctic cirrus solar radiative effects in the Integrated Forecasting System with airborne measurements. Atmos. Chem. Phys., 24, 8085--8104. doi:https://doi.org/10.5194/acp-24-8085-2024, 2024.

Schäfer, M., Wolf, K., Ehrlich, A., Hallbauer, C., Jäkel, E., Jansen, F., . . . Wendisch, M.: VELOX – a new thermal infrared imager for airborne remote sensing of cloud and surface properties. Atmos. Meas. Tech., 15(5), 1491-1509. doi:10.5194/amt-15-1491-2022, 2022.

Schäfler, A., and Coauthors:. The North Atlantic Waveguide and Downstream Impact Experiment. Bulletin of the American Meteorological Society, 99, 1607--1637. doi:https://doi.org/10.1175/BAMS-D-17-0003.1, 2018.

Sourdeval, O., Gryspeerdt, E., Krämer, M., Goren, T., Delanoë, J., Afchine, A., . . . Quaas, J.: Ice crystal number concentration estimates from lidar–radar satellite remote sensing – Part 1: Method and evaluation. Atmos. Chem. Phys., 18, 14327--14350. doi: https://doi.org/10.5194/acp-18-14327-2018, 2018.

Stephens, G. L., Vane, D. G., S, T., Im, E., Durden, S., Rokey, M., . . . Marchand, R.: CloudSat mission: Performance and early science after the first year of operation. Journal of Georphysical Research: Atmosphere, 113(D8). doi: https://doi.org/10.1029/2008JD009982, 2008.

Stephens, G., Winker, D., Pelon, J., Trepte, C., Vane, D., Yuhas, C., . . . Lebsock, M.:. CloudSat and CALIPSO within the A-Train: Ten Years of Actively Observing the Earth System. Bulletin of the American Meteorological Society, 569--581. doi:https://doi.org/10.1175/BAMS-D-16-0324.1., 2018.

Stevens, B., Ament, F., Bony, S., Crewell, S., Ewald, F., Gross, S., . . . Farrell, D.: A High-Altitude Long-Range Aircraft Configured as a Cloud Observatory: The NARVAL Expeditions. Bullentin of the American Meteorological Society, 100(6), 1061-1077, https://journals.ametsoc.org/view/journals/bams/100/6/bams-d-18-0198.1.xml, 2019.

Stevens, B., Bony, S., Gross, S., Klocke, D., Windmiller, J., Wing, A. A., . . . Wu, Y.: ORCESTRA: Organized Convection and EarthCARE Studies over the Tropical Atlantic. Tellus B, in review, 2026

Stevens, B., Farrell, D., Hirsch, L., Jansen, F., Nuijens, L., Serikov, I., . . . Prospero, J. M.: The Barbados Cloud Observatory: Anchoring Investigations of Clouds and Circulation on the Edge of the ITCZ. Bulletin of the American meteorological Society, 97(5), 787--801. doi:https://doi.org/10.1175/BAMS-D-14-00247.1, 2016.

Urbanek, B., Groß, S., Schäfler, A., and Wirth, M.: Determining stages of cirrus evolution: a cloud classification scheme. Atmos. Meas. Tech., 10, 1653–1664, 2017.

Volkmer, L., Kölling, T., Zinner, T., and Mayer, B.: Consideration of the cloud motion for aircraft-based stereographically derived cloud geometry and cloud top heights. Atmos. Meas. Tech., 17, 6807--6817. doi:https://doi.org/10.5194/amt-17-6807-2024, 2024.

Wandinger, U., Floutsi, A. A., Baars, H., Haarig, M., Ansmann, A., Hünerbein, A., . . . Cole, J.: HETEAC – the Hybrid End-To-End Aerosol Classification model for EarthCARE. Atmos. Meas. Tech., 16, 2485--2510. doi:https://doi.org/10.5194/amt-16-2485-2023, 2023.

Wandinger, U., Haarig, M., Baars, H., Donovan, D., and van Zadelhoff, G.-J.: Cloud top heights and aerosol layer properties from EarthCARE lidar observations: the A-CTH and A-ALD products. Atmos. Meas. Tech., 16, 4031--4052. doi:https://doi.org/10.5194/amt-16-4031-2023, 2023.

Weber, A., Kölling, T., Pörtge, V., Baumgartner, A., Rammeloo, C., Zinner, T., and Mayer, B.:. Polarization upgrade of specMACS: calibration and characterization of the 2D RGB polarization-resolving cameras. Atmos. Meas. Tech., 17, 1419--1439. doi:https://doi.org/10.5194/amt-17-1419-2024, 2024.

Weber, A., Pörtge, V., Emde, C., and Mayer, B.: Retrieval of cloud thermodynamic phase partitioning from multi-angle polarimetric imaging of Arctic mixed-phase clouds, Atmos. Meas. Tech., 18, 7581–7601, https://doi.org/10.5194/amt-18-7581-2025, 2025.

Wehr, T., Kubota, T., Tzeremes, G., Wallace, K., Nakatsuka, H., Ohno, Y., . . . Bernaerts, D.: The EarthCARE mission – science and system overview. Atmos. Meas. Tech.s, 16(15), 3581--3608. doi:https://doi.org/10.5194/amt-16-3581-2023, 2023.

Weinzierl, B., Sauer, D., Esselborn, M., Petzold, A., Veira, A., Rose, M., . . . Freuntenthaler, V.: Microphysical and optical properties of dust and tropical biomass burning aerosol layers in the Cape Verde region—an overview of the airborne in situ and lidar measurements during SAMUM-2. Tellus B: Chemical and Physical meteorology, 4, 589--618. doi:https://doi.org/10.1111/j.1600-0889.2011.00566.x, 2011.

Winker, D. M., Pelon, J., Coakley, J. A., Ackerman, S. A., Charlson, R. J., Colarco, P. R., . . . Wielicki: The Calipso Mission: A Global 3D View of Aerosols and Clouds. Bulletin of the American Meteorological Society, 91(9), 1211--1230. doi:https://doi.org/10.1175/2010BAMS3009.1, 2010.

Wirth, M., Fix, A., Mahnke, P., Schwarzer, H., Schrandt, F., and Ehret, G.: The airborne multi-wavelength water vapor differential absorption lidar WALES: system design and performance. Applied Physics B, 96, 201-213. doi:10.1007/s00340-009-3365-7, 2009.

Witschas, B., Lemmerz, C., Geiß, A., Lux, O., Marksteiner, U., Rahm, S., . . . Weiler, F.: First validation of Aeolus wind observations by airborne Doppler wind lidar measurements. Atmos. Meas. Tech., 13, 2381--2369. doi:https://doi.org/10.5194/amt-13-2381-2020, 2020.

Witschas, B., Lemmerz, C., Geiß, A., Lux, O., Marksteiner, U., Rahm, S., . . . Weiler, F.: Validation of the Aeolus L2B wind product with airborne wind lidar measurements in the polar North Atlantic region and in the tropics. Atmos. Meas. Tech., 15, 7049--7070. doi:https://doi.org/10.5194/amt-15-7049-2022, 2022.

Wolf, K., Ehrlich, A., Mech, M., Hogan, R. J., and Wendisch, M.: Evaluation of ECMWF Radiation Scheme Using Aircraft Observations of Spectral Irradiance above Clouds. Journal of Atmospheric Science, 77, 2665--2685. doi:https://doi.org/10.1175/jas-d-19-0333.1, 2020.

Appendix A: PACE-Validation

The focus of the PERCUSION campaign was clearly on the validation of EarthCARE. However, our flight schedule and measurement strategy allowed also to underfly NASA's PACE (Plankton, Aerosol, Cloud, ocean Ecosystem) mission during four measurement flights out of Barbados. PACE (NASA PACE - Home) was launched on 8 February 2024 and aims to extend the data record of ocean colour, aerosol and cloud data for Earth systems studies as well as to address new and emerging science questions. For that, PACE is equipped with the Ocean Color Instrument (OCI) and the Multi-angle Polarimeters HARP2 and SPEXone. The maximum swath width is about 2500 km for the OCI, 1500 km for HARP2, and 100 km for SPEXone. Any measurements within the swath width of the satellite are thus valuable for validation. Figure A1 gives an overview of the flight scene from a lidar perspective for the different days a underpass was performed or HALO was measuring within the swath of PACE. Over measurements covered a variety of different conditions from background marine aerosol conditions, over midlevel stratiform clouds, thin cirrus condition, cirrus clouds, to clouds of deep convective systems. With that our measurements not only serve for direct comparisons of the polarimeter measurements using the specMACS data, but also for the verification of the atmospheric model to investigate the impact of aerosol and clouds on PACE measurements. For the latter especially the vertical information from lidar and radar as well as their synergistic use to derive microphysical cloud properties is of interest. Table A1 gives information on dates and times of the underpasses.

Table A1: Information of date, time and location of HALO measurements along or in the PACE tack.

Date	Best Match Time (UTC)	Time on track (UTC)	Best Match Distance (km)
7 September 2024	16 :00	17:10 – 17:39	89.9
16 September 2024	16 :15	16:02 – 16:43	1.0
19 September 2024	16 :22	15:45 – 16:27	0.6
28 September 2024	16 :35	16:23 – 17:30	21.5

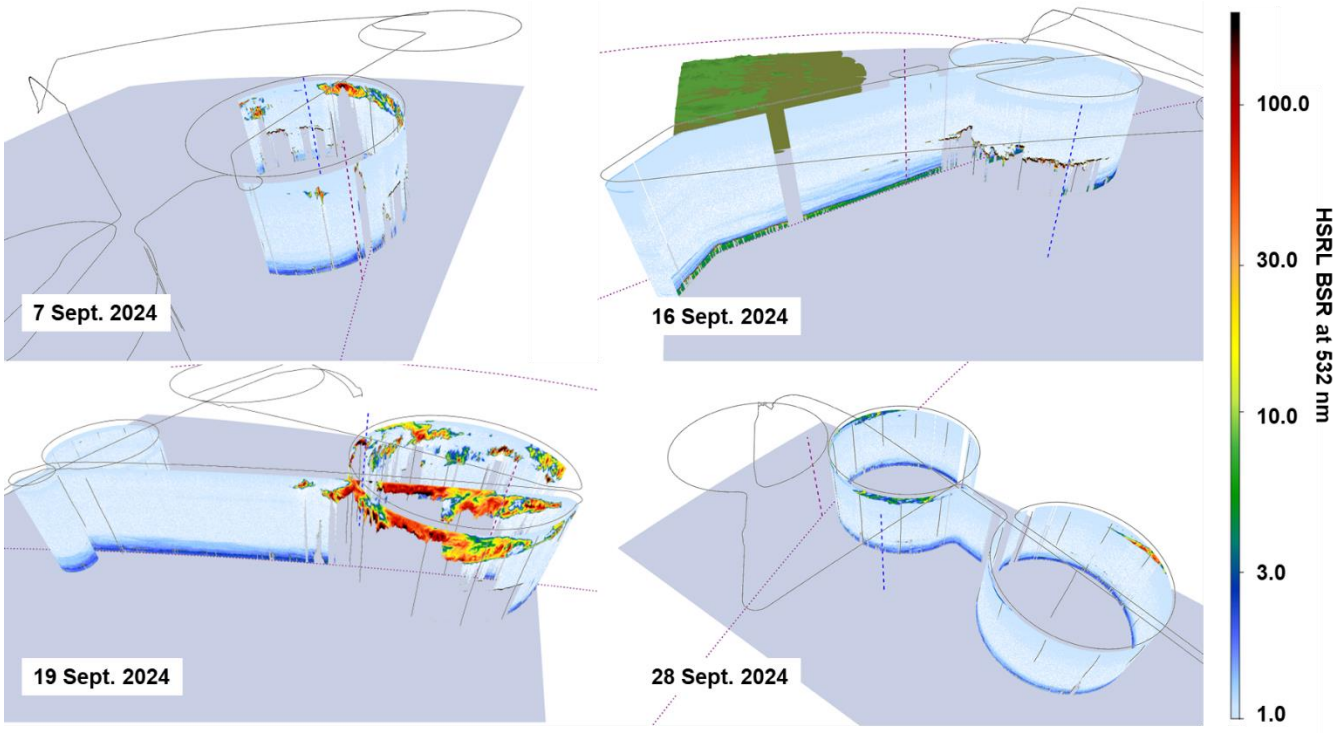

Figure A1: Cross-section of the backscatter ratio at 532 nm from WALES measurements for the four underpasses within the PACE track. The dashed red lines indicate the nearest PACE measurement in time, the blue dashed line indicate the nearest EarthCARE measurement in time.

Appendix B: Bridging the gap from CALIPSO/Cloudsat to EarthCARE

CALIPSO and Cloudsat provided a large opportunity to study aerosol, clouds, their interaction and their impact on radiation and precipitation. This will be continued with EarthCARE. However, going from CALIPSO/Cloudsat to EarthCARE, we do not only have a change in lidar wavelength and technique, but also a change in sensitivity and resolution for both, lidar and radar. Unfortunately, both satellite constellations did not have a direct overlap, making it difficult to directly link the two time-series and data sets. Collocated measurements with both, the CALIPSO/Cloudsat constellation and with EarthCARE, are needed to bridge that gap. Next to continuing ground-based lidar and radar measurements, which provide long-term measurements but with limited overlap, collocated airborne measurements with lidar and radar provide a valuable contribution. The largest number of CALIPSO underflights is certainly provided by the NASA Langley lidar group with their HSRL/HSRL-2 system (Hair et al., 2006). After the launch of EarthCARE, they also performed EarthCARE underpasses for the validation of the ATLID. However, our combined active (lidar and radar) and passive remote sensing payload (Stevens, et al., 2019) bridges both satellite missions with correlative airborne lidar and radar measurements underflying both CALIPSO/CloudSat and EarthCARE. The basic lidar and radar products are analyzed and available as two combined datasets for WALES lidar data and MIRA cloud radar data from A-Train underflights with HALO via Zenodo (Ewald and Wirth, 2026; Ewald, 2026).

980 Table B1: Information on date, region, time flight mission and measurement conditions for CALIPSO/Cloudsat underpasses with the same lidar and radar instruments used during PERCUSION.

Date	Flight region	Time of collocation [UTC]	Flight mission	Condition
24 Jul. 2013	Germany	12:18	NARVAL (test)	Thin cirrus clouds Continental background aerosol
10 Dec. 2013	North Atlantic	15:08	NARVAL (south)	Low level precipitating clouds Marine aerosol
11 Dec. 2013	Sub-tropical North Atlantic	17:26	NARVAL (south)	Marine aerosol Shallow marine convection
12 Dec 2013	Sub-tropical North Atlantic	16:30	NARVAL (south)	Marine aerosol Shallow and stratiform clouds
14 Dec. 2013	Sub-tropical North Atlantic	16:18	NARVAL (south)	Marine aerosol Shallow convection, partly precipitating
15 Dec. 2013	Sub-tropical North Atlantic	17:01	NARVAL (south)	Marine aerosol Shallow convection, partly precipitating
16 Dec. 2013	Sub-tropical North Atlantic	16:07	NARVAL (south)	Marine aerosol Shallow convection, partly precipitating
20 Dec. 2013	North Atlantic	17:23	NARVAL (south)	Marine aerosol Shallow convection
9 Jan. 2014	Extra-tropical North Atlantic	15:29	NARVAL (north)	Marine aerosol Scattered low level clouds, partly precipitating
18 Jan. 2014	Extra-tropical North Atlantic	13:44	NARVAL (north)	Deep convective clouds, ice anvils, frontal bands
21 Jan. 2014	Extra-tropical North Atlantic	14:19	NARVAL (north)	High and convective clouds Marine aerosol
10 Aug. 2016	Sub-tropical North Atlantic	17:09	NARVAL-II	Low to mid-level clouds, partly precipitating Marine aerosol and Saharan dust
15 Aug. 2016	Sub-tropical North Atlantic	17:10	NARVAL-II	Stratiform and upper-level clouds Marine aerosol and Saharan dust
17 Aug. 2016	Sub-tropical North Atlantic	17:01	NARVAL-II	Low level and cirrus clouds Marine aerosol and dust mixture
19 Aug. 2016	Sub-tropical North Atlantic	16:47	NARVAL-II	Shallow marine convection Marine aerosol, Saharan dust and dust mixture
14 Oct. 2016	Extra-tropical North Atlantic	12:53	NAWDEX	Deep convection, precipitation, stratiform clouds Marine aerosol